

Accepted Manuscript

N-Propargylpiperidines with Naphthalene-2-Carboxamide or Naphthalene-2-Sulfonamide Moieties: Potential Multifunctional Anti-Alzheimer's Agents

Urban Košak, Damijan Knez, Nicolas Coquelle, Boris Brus, Anja Pišlar, Florian Nachon, Xavier Brazzolotto, Janko Kos, Jacques-Philippe Colletier, Stanislav Gobec

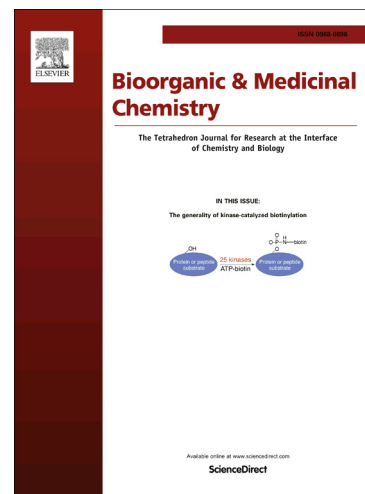
PII: S0968-0896(16)30909-9
DOI: <http://dx.doi.org/10.1016/j.bmc.2016.11.032>
Reference: BMC 13399

To appear in: *Bioorganic & Medicinal Chemistry*

Received Date: 6 October 2016
Revised Date: 14 November 2016
Accepted Date: 17 November 2016

Please cite this article as: Košak, U., Knez, D., Coquelle, N., Brus, B., Pišlar, A., Nachon, F., Brazzolotto, X., Kos, J., Colletier, J.-P., Gobec, S., *N*-Propargylpiperidines with Naphthalene-2-Carboxamide or Naphthalene-2-Sulfonamide Moieties: Potential Multifunctional Anti-Alzheimer's Agents, *Bioorganic & Medicinal Chemistry* (2016), doi: <http://dx.doi.org/10.1016/j.bmc.2016.11.032>

This is a PDF file of an unedited manuscript that has been accepted for publication. As a service to our customers we are providing this early version of the manuscript. The manuscript will undergo copyediting, typesetting, and review of the resulting proof before it is published in its final form. Please note that during the production process errors may be discovered which could affect the content, and all legal disclaimers that apply to the journal pertain.



***N*-Propargylpiperidines with Naphthalene-2-Carboxamide or Naphthalene-2-Sulfonamide Moieties: Potential Multifunctional Anti-Alzheimer's Agents**

Urban Košak,[‡] Damijan Knez,[‡] Nicolas Coquelle,[§] Boris Brus,[‡] Anja Pišlar,[‡] Florian Nachon,[°] Xavier Brazzolotto,[°] Janko Kos,[‡] Jacques-Philippe Colletier,[§] Stanislav Gobec^{‡,}*

[‡]Faculty of Pharmacy, University of Ljubljana, Aškerčeva 7, 1000 Ljubljana, Slovenia

[§]Institut de Biologie Structurale, Univ. Grenoble Alpes, CEA, CNRS, 38044 Grenoble, France

[°] Institut de Recherche Biomédicale des Armées, 91223 Brétigny-sur-Orge, France

***Corresponding Author:** Stanislav Gobec

Faculty of Pharmacy, University of Ljubljana, Aškerčeva 7, 1000 Ljubljana, Slovenia

Tel: +386-1-4769500; Fax: +386-1-4258031; E-mail: stanislav.gobec@ffa.uni-lj.si

Abbreviations

A β , amyloid β ; ACh, acetylcholine; mAChE, murine acetylcholinesterase; AD, Alzheimer's disease; BBB, blood-brain barrier; hBChE, human butyrylcholinesterase; ChE(s), cholinesterase(s); FAD, flavine adenine dinucleotide; hMAO-A, human monoamine oxidase A; hMAO-B, human monoamine oxidase B; MTDL, multitarget-directed ligand; MTS, (3-(4,5-dimethylthiazol-2-yl)-5-(3-carboxymethoxyphenyl)-2-(4-sulfophenyl)-2*H*-tetrazolium, inner salt); PAMPA, parallel artificial membrane permeation assay; TFA, 2,2,2-trifluoroacetic acid.

ABSTRACT

In the brains of patients with Alzheimer's disease, the enzymatic activities of butyrylcholinesterase (BChE) and monoamine oxidase B (MAO-B) are increased. While BChE is a viable therapeutic target for alleviation of symptoms caused by cholinergic hypofunction, MAO-B is a potential therapeutic target for prevention of neurodegeneration in Alzheimer's disease. Starting with piperidine-based selective human (h)BChE inhibitors and propargylamine-based MAO inhibitors, we have designed, synthesized and biochemically evaluated a series of *N*-propargylpiperidines. All of these compounds inhibited hBChE with good selectivity over the related enzyme, acetylcholinesterase, and crossed the blood-brain barrier in a parallel artificial membrane permeation assay. The crystal structure of one of the inhibitors (compound **3**) in complex with hBChE revealed its binding mode. Three compounds (**4**, **5**, **6**) showed concomitant inhibition of MAO-B. Additionally, the most potent hBChE inhibitor **7** and dual BChE and MAO-B inhibitor **6** were non-cytotoxic and protected neuronal SH-SY5Y cells from toxic amyloid β -peptide species.

Keywords: multitarget-directed ligands; butyrylcholinesterase inhibitors; MAO-B inhibitors; Alzheimer's disease.

INTRODUCTION

Alzheimer's disease (AD) is a neurodegenerative disorder that is characterized by progressive deterioration of memory and other cognitive functions. Neurodegeneration and synaptic dysfunction caused by accumulation of the aggregated amyloid β -peptide ($A\beta$) and hyperphosphorylated protein tau, and by oxidative stress [1] severely affect the cholinergic system [2]. As a result, the levels of the neurotransmitter acetylcholine (ACh) are severely decreased [3]. This produces memory and cognitive deficits [4], which are distinctive for patients with AD. Inhibition of ACh hydrolysis in the brain is thus used to restore cognitive functions and alleviate symptoms of AD.

Two cholinesterases (ChEs) terminate cholinergic neurotransmission through their catalysis of the hydrolysis of ACh: acetylcholinesterase (AChE) and butyrylcholinesterase (BChE) [5]. Three out of the four approved drugs for the treatment of AD are AChE inhibitors (Figure 1A, donepezil [6], galantamine [7] and rivastigmine [8]); however, these have limitations due to undesired AChE inhibition in the peripheral and autonomous nervous systems that can produce adverse cholinergic side effects. This necessitates limited dosing, and can result in limited clinical efficacy in advanced stages of the disease [9]. These limitations can be overcome by selective inhibition of BChE [10]–[12], because as AD progresses, the enzymatic activity of BChE in the brain increases [10]. This makes BChE a prospective therapeutic target in AD, with one selective BChE inhibitor (Figure 1B, a cymserine analog [11]) successfully advanced to Phase I clinical trials.

Monoamine oxidase (MAO) is one of the several proteins that contribute to oxidative stress in AD [13]. MAO is a flavine adenine dinucleotide (FAD)-containing enzyme that is located in the outer mitochondrial membrane [14]. In most mammalian tissues, two isoenzymes are present: MAO-A and MAO-B [13]. In the brains of patients with AD, the enzymatic activity of MAO-B is increased [13]–[16], which results in increased levels of

oxidative deamination reaction products such as hydrogen peroxide, ammonia and aldehydes; these then contribute to neurodegeneration [13],[15],[16]. Selective inhibition of MAO-B in the brain might thus be useful for the management of AD [13]–[16]. Accordingly, MAO-B inhibitors (Figure 1C) are currently in clinical trials for the treatment of AD [13],[14],[16]. MAO inhibitory activity has also been combined with ChE inhibitory activity in multitargeting compounds (Figure 1D) that use the multitarget-directed ligand (MTDL) approach. Several multitarget compounds are currently being examined in preclinical and clinical trials [13],[15],[17][19].

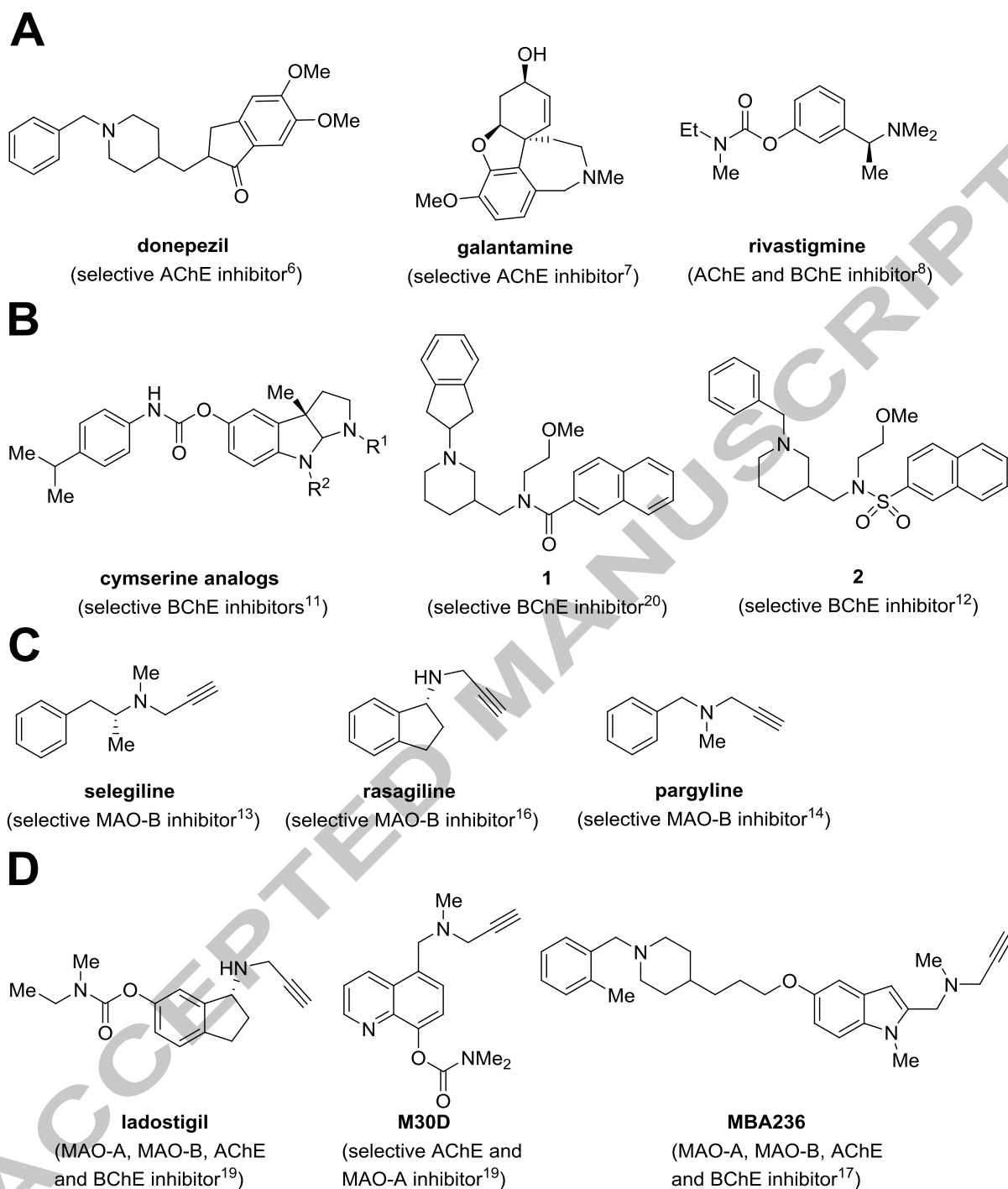


Figure 1. Structures of the currently approved ChE inhibitors for the treatment of Alzheimer's disease (A), the selective BChE inhibitors (B), the selective MAO-B inhibitors (C), and the multitarget-directed ligands that use ChE and MAO inhibitory activities (D).

Recently, we described a novel piperidine-3-ylmethanamine-based selective human (h)BChE inhibitor **1** (Figure 1B) that showed reversible, slow-tight binding inhibition with

low nanomolar IC_{50} [20]. The structure of this inhibitor has already been used to develop an *in-vivo* active sulfonamide derivative **2** (Figure 1B)[12]. Additionally, compounds **1** and **2** can protect neuronal cells from the toxic $A\beta_{1-42}$ species. In the current study, our hypothesis was that replacing *N*-piperidine substituents of our neuroprotective selective hBChE inhibitors **1** and **2** with the propargyl moiety of selective irreversible propargylamine MAO-B inhibitors would produce selective hBChE and MAO-B inhibitors with neuroprotective activity.

We report here the design, synthesis, and biochemical evaluation of a series of *N*-propargylpiperidine derivatives, as potent inhibitors of hBChE. The crystal structure of compound **3** in complex with hBChE reveals its binding mode. Additionally, three of these compounds (**4–6**) inhibit MAO-B, which demonstrates the feasibility of dual inhibition of hBChE and MAO-B using a single compound. Furthermore, two compounds (**6, 7**) protect neuronal cells from the toxic $A\beta_{1-42}$ species. Hence, *N*-propargylpiperidines represent a new class of drug candidates for symptomatic treatment of AD.

RESULTS AND DISCUSSION

Design

The crystal structure of compound **1** in complex with hBChE and the chemical structures of selective irreversible propargylamine MAO-B inhibitors (e.g., selegiline, rasagiline) were used as the starting point to design the *N*-propargylpiperidines (Figure 2). It was essential that this design produced compounds with drug-like properties [21]. Selegiline and rasagiline contain a propargylamine moiety that has been shown to covalently bind to the *N5* atom of the flavine ring of the FAD cofactor [13],[14]. The piperidine nitrogen in hBChE inhibitor hit compound **1** was recognized as the most suitable functional group for the simple introduction of the propargyl moiety [22], and thus for the design of novel piperidine-based propargylamines.

Previous studies on derivatives of hit compound **1** have revealed that the naphthalene-2-yl moiety is essential for good inhibitory potency, due to its tight binding in the acyl binding pocket of hBChE [12]. Accordingly, all of the *N*-propargylpiperidines designed here retained the naphthalene-2-yl moiety of the parent hit compound **1**. Sulfonamides were designed to explore how the bioisosteric replacement of a carboxamide with a sulfonamide [23] affects ChE and MAO inhibition. The role of the *N*-alkyl chain of these inhibitors (Figure 2, **R**) was studied by its removal or elongation. We removed the *N*-alkyl chain and designed compounds with a lower molecular weight and a reduced number of rotatable bonds. This is a common design strategy in medicinal chemistry that has been used to improve brain exposure of drug candidates [24]. (CH₂)₂OMe was kept as the substituent **R** to directly study the effects of replacing the 2,3-dihydro-1H-inden-2-yl of hit compound **1** and benzyl group of compound **2** with the propargylamine moiety on the inhibitory potency and selectivity against hBChE, and Aβ1–42-anti-aggregation activity. To investigate the effects of an additional methylene group in the *N*-alkyl chain on ChE inhibition, MAO inhibition and Aβ1–42-anti-aggregation activity of compounds with the (CH₂)₃OMe group were also designed. Finally, 1,4-disubstituted piperidine derivatives were designed to examine the effects of the piperidine ring disubstitution pattern on ChE and MAO inhibition (Figure 2).

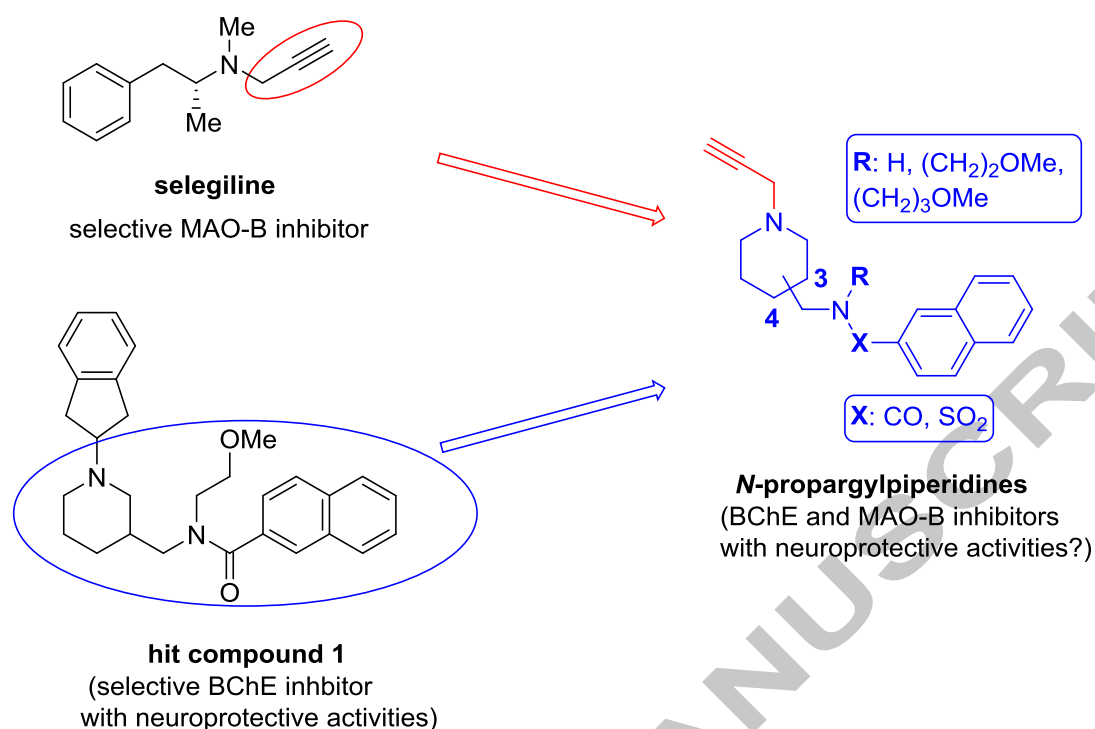
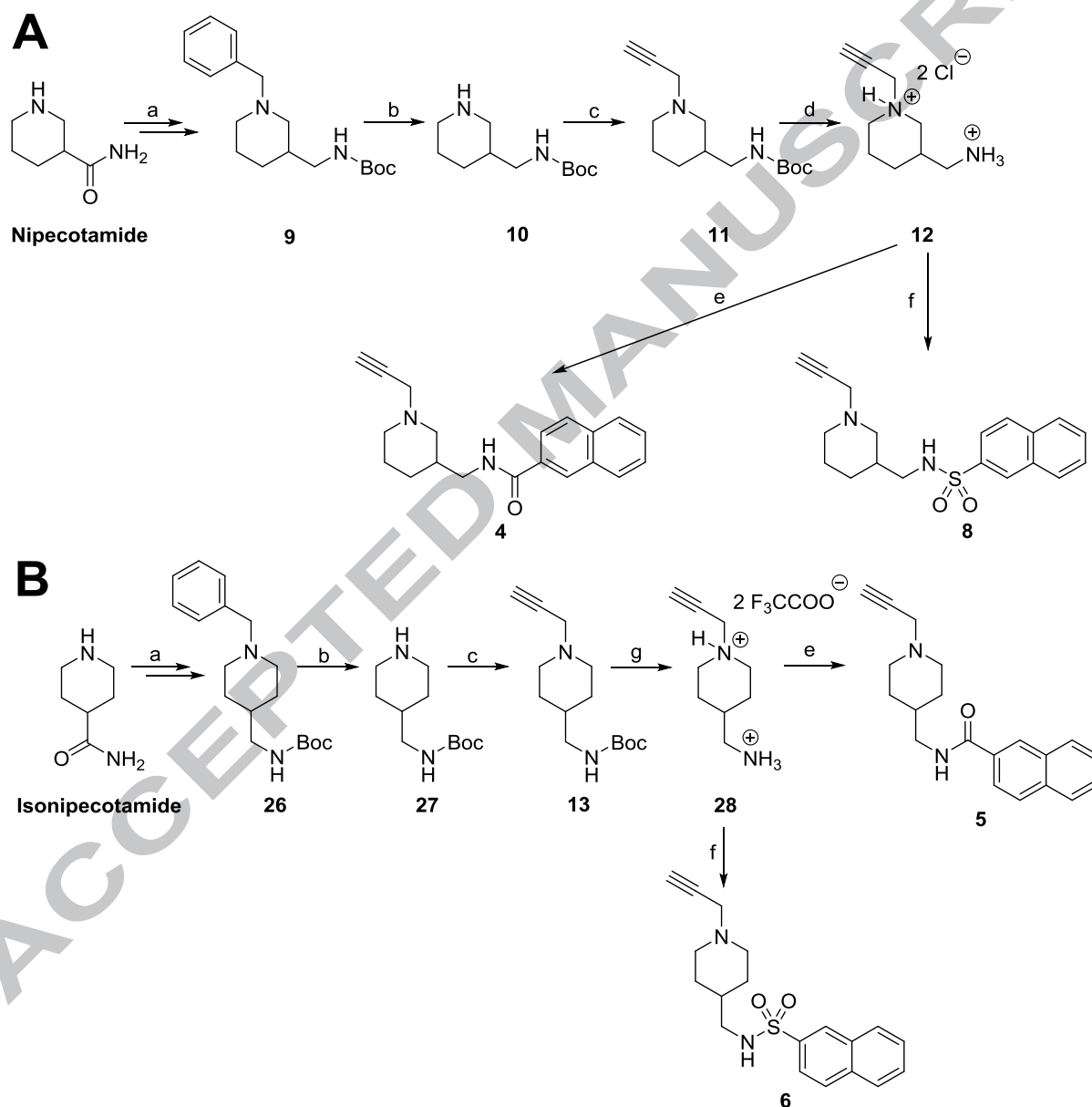


Figure 2. Design of the *N*-propargylpiperidines.

Synthesis

The synthesis of 1,3-disubstituted piperidines without the *N*-alkyl chain **4** and **8** is presented in Scheme 1A. The key intermediate, orthogonally protected piperidin-3-ylmethanamine **9** was prepared from commercially available nipecotamide using a straightforward two step procedure, as previously reported [25]. In the next step, the *N*-benzyl group of **9** was removed using cyclohexene in the presence of catalytic amount of Pearlman's catalyst (palladium hydroxide on carbon) to provide crude secondary amine **10** [26], which was then reacted with propargyl bromide in the presence of Cs₂CO₃ in acetone [27], to produce propargyl amine **11**. The *tert*-butyloxycarbonyl protecting group from compound **11** was removed using HCl solution in Et₂O since using TFA in CH₂Cl₂ produced an impure desired product. The crude amine dihydrochloride **12** was then reacted with 2-naphthoyl chloride or naphthalene-2-sulfonyl chloride, to produce amide **4** or sulfonamide **8**, respectively.

The synthesis of 1,4-disubstituted piperidines without the *N*-alkyl chain **5** and **6** is presented in Scheme 1B. They were prepared from commercially available isonipecotamide using the same reagents and conditions used to synthesize inhibitors **4** and **8** from nipecotamide, with the exception that the butyloxycarbonyl protecting group from compound **13** was removed using TFA in CH_2Cl_2 which, in this case produced the pure desired product.

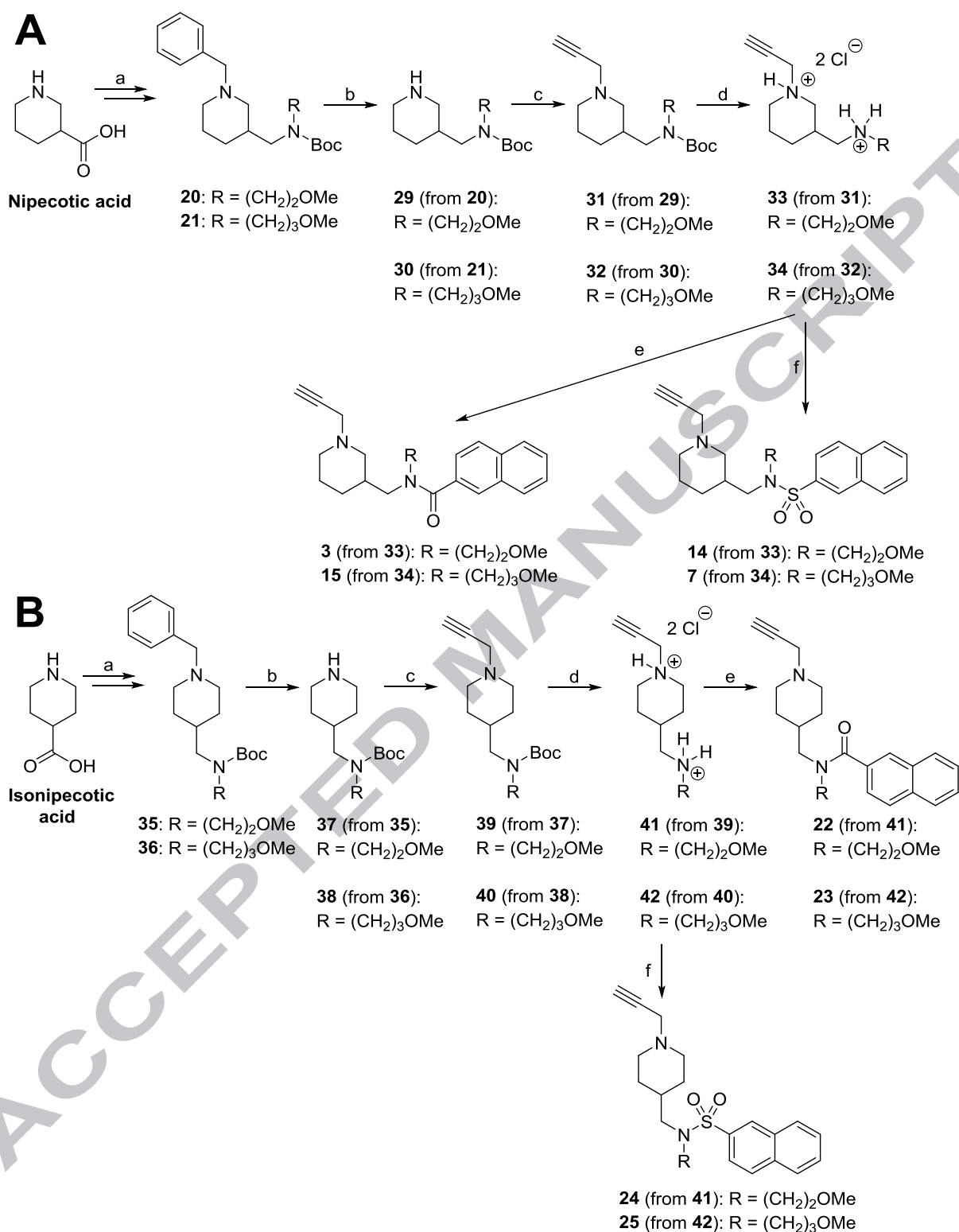


Scheme 1. Reagents and conditions: (a) (i) PhCOCl , Et_3N , THF, 0°C to rt, 22–25 h; (ii) LiAlH_4 , anhydrous THF, rt to reflux, under argon, 2–3 h, (iii) Boc_2O , Et_3N , CH_2Cl_2 , 0°C to rt, 21–24 h, (48–78% overall yield); (b) cyclohexene, $\text{Pd}(\text{OH})_2/\text{C}$ cat., MeOH, rt, under argon, 20 h (90–91%); (c) propargyl bromide (80 wt. % solution in toluene), Cs_2CO_3 , acetone, rt, 24 h (58–75%); (d) 2 M HCl

solution in Et₂O, MeOH, 0 °C to rt, under argon, 24 h (99%); (e) 2-naphthoyl chloride, Et₃N, CH₂Cl₂, 0 °C to rt, 24 h (78–91%); (f) naphthalene-2-sulfonyl chloride, Et₃N, CH₂Cl₂, 0 °C to rt, 24 h (81–82%); (g) TFA, CH₂Cl₂, rt, 24 h (97%).

The synthesis of 1,3-disubstituted piperidines with the *N*-alkyl chain **3**, **7**, **14** and **15** is presented in Scheme 2A. Commercially available nipecotic acid was first converted into orthogonally protected piperidin-3-ylmethanamines **20** and **21** using a two-step procedure, as previously reported [25]. Amine **20** was then converted into amide **3** and sulfonamide **14**, while amine **21** was converted into amide **15** and sulfonamide **7** using the same reagents and conditions used to synthesize inhibitors **4** and **8** in Scheme 1A.

1,4-Disubstituted piperidines with *N*-alkyl chain **22–25** were synthesized from commercially available isonipecotic acid using the same reagents and conditions used to synthesize inhibitors **3**, **7**, **14** and **15** (Scheme 2B).



Scheme 2. Reagents and conditions: (a) (i) PhCOCl, K₂CO₃, THF–H₂O, 0 °C to rt, 22 h, (ii) 6 M HCl (aq), 0 °C; (iii) H₂N-R, TBTU, Et₃N, CH₂Cl₂, rt, 21–23h; (iv) LiAlH₄, anhydrous THF, rt to reflux, under argon, 2–3 h, (v) Boc₂O, Et₃N, CH₂Cl₂, 0 °C to rt, 17–22 h, (56–74% overall yield); (b) cyclohexene, Pd(OH)₂/C cat., MeOH, rt, under argon, 20 h (94–99%); (c) propargyl bromide (80 wt.

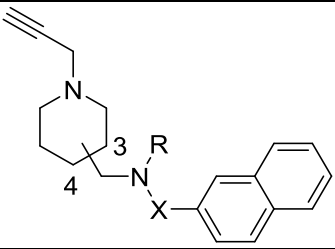
% solution in toluene), Cs_2CO_3 , acetone, rt, 24 h (64–78%); (d) 2 M HCl solution in Et_2O , MeOH, 0 °C to rt, under argon, 24 h (93–97%); (e) 2-naphthoyl chloride, Et_3N , CH_2Cl_2 , 0 °C to rt, 24 h (92–96%); (f) naphthalene-2-sulfonyl chloride, Et_3N , CH_2Cl_2 , 0 °C to rt, 24 h (79–97%).

In-Vitro Enzyme Inhibition and Structure-Activity Relationships

The inhibitory potencies against hBChE and murine (m)AChE for these *N*-propargyl piperidines were determined using the method of Ellman [28], with all of these compounds showing selectivity toward hBChE over mAChE (Table 1).

The inhibitory potencies against human (h)MAO-A and hMAO-B were determined for all of the target compounds, using a previously described fluorescence-based Amplex Red assay [17] with minor modifications. Table 1 reports the structures and inhibitory potencies of these *N*-propargyl piperidines. All of these compounds showed moderate selectivity toward hMAO-B over hMAO-A (Table 1), and three showed IC_{50} values ranging from 53.9 μM to 72.6 μM against hMAO-B.

Table 1. Inhibitory potencies and structures of *N*-propargyl piperidines, tacrine, clorgyline, and pargyline.



Compound number or name	Pdp ^a	R	X	hBChE IC ₅₀ ±SEM (μM)	mAChE IC ₅₀ ±SEM (μM)	Selectivity ratio IC ₅₀ mAChE/IC ₅₀ hBChE	hMAO-A ^b IC ₅₀ (μM)	hMAO-B ^b IC ₅₀ ±SEM (μM)	Selectivity ratio IC ₅₀ hMAO-A/IC ₅₀ hMAO-B
4	1,3	H	CO	23.444 ±1.497	>100	>4.27	>100	59.293 ±0.002	>1.69
3	1,3	(CH ₂) ₂ OMe	CO	3.306 ±0.381	>100	>30.25	>100	>100	1
15	1,3	(CH ₂) ₃ OMe	CO	8.641 ±1.989	>100	>11.57	>100	>100	1
5	1,4	H	CO	54.396 ±9.428	>100	>1.84	>100	72.611 ±1.668	>1.38
22	1,4	(CH ₂) ₂ OMe	CO	4.040 ±0.237	>100	>24.75	>100	>100	1
23	1,4	(CH ₂) ₃ OMe	CO	4.590 ±0.230	>100	>21.79	>100	>100	1
8	1,3	H	SO ₂	1.223 ±0.036	>100	>81.77	>100	>100	1
14	1,3	(CH ₂) ₂ OMe	SO ₂	0.137 ±0.003	>100	>729.93	>100	>100	1
7	1,3	(CH ₂) ₃ OMe	SO ₂	0.127 ±0.006	>100	>787.40	>100	>100	1
6	1,4	H	SO ₂	2.600 ±0.348	>100	>38.46	>100	53.904 ±4.781	>1.86
24	1,4	(CH ₂) ₂ OMe	SO ₂	0.384 ±0.017	>100	>260.42	>100	>100	1
25	1,4	(CH ₂) ₃ OMe	SO ₂	0.281 ±0.024	>100	>355.87	>100	>100	1
Tacrine	/	/	/	0.023 ±0.003	0.115 ±0.009	5	not tested	not tested	/
Clorgyline	/	/	/	not tested	not tested	/	0.0034 ±0.0003	13.568 ±1.157	0.00025
Pargyline	/	/	/	not tested	not tested	/	3.368 ±0.275	0.195 ±0.019	17.27

^apdp = piperidine disubstitution pattern

^bdetermined after 15 min preincubation of inhibitor with the enzyme

As propargylamines inhibit MAO irreversibly by forming covalent *N*(5)-flavocyanine adducts [13],[14] we performed the reversibility test [17] with compound **6** to determine the mechanism of hMAO-B inhibition. The results of the 100-fold dilution assay showed that this inhibitor binds irreversibly, maintaining over 70% inhibition after dilution of the preincubated mixture (Figure 3). The time-dependent mechanism of inhibition was confirmed in the IC₅₀ shift assay, as the IC₅₀ decreased with prolongation of incubation time (Figure 4).

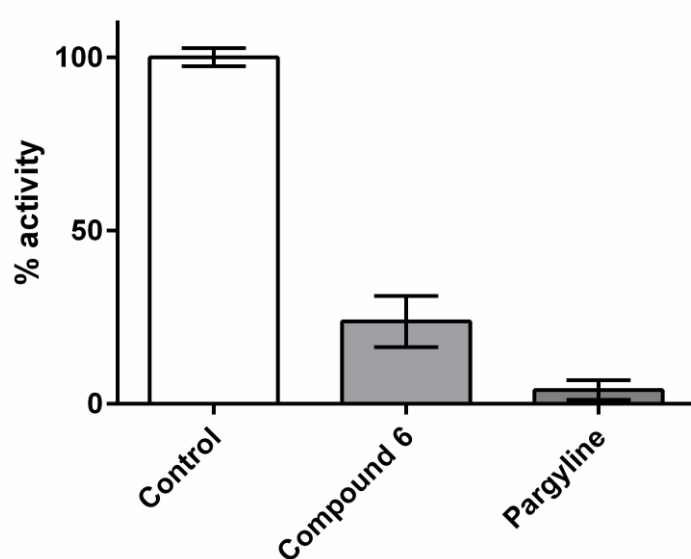


Figure 3. Recovery of hMAO-B activity after 100-fold dilution following 15 min incubation (at 37 °C) of the 100× enzyme concentration with 10-fold the IC₅₀ of compound **6** and pargyline. The control was carried out in the absence of inhibitor and diluted in the same way. Data are expressed as percentages of control ±SEM of four independent experiments.

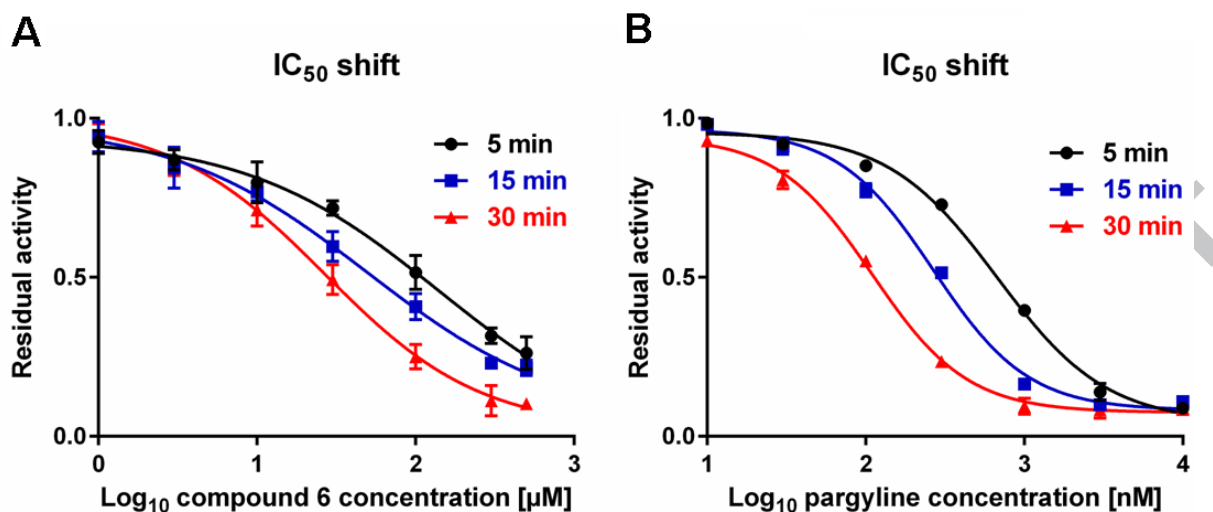


Figure 4. The shifted IC₅₀ curves for compound 6 (A) and pargyline (positive control) (B) at various pre-incubation times indicate time-dependent inhibition of hMAO-B.

The most important findings regarding the structure–activity relationships are summarized in Figure 5. Replacing the 2,3-dihydro-1*H*-inden-2-yl and benzyl groups on the piperidine nitrogen with the propargylamine moiety reduced the inhibitory potency against hBChE [12],[20]. The *N*-propargylpiperidine sulfonamides were more potent hBChE inhibitors compared to their analogous carboxamides. Removal of the *N*-alkyl chain [(CH₂)_nOMe] from the carboxamide and sulfonamide nitrogen reduced the inhibitory potency, as secondary carboxamides and sulfonamides were significantly weaker inhibitors than their tertiary counterparts. Elongation of the *N*-alkyl chain with an additional methylene group did not affect the inhibitory potency significantly. Analogous to sulfonamide derivatives of hit compound 1 [12], 1,3 disubstituted *N*-propargylpiperidines were more potent hBChE inhibitors than their 1,4 disubstituted counterparts. The most potent hBChE inhibitor of the series, compound 7 (IC₅₀ = 127 nM) is thus a 1,3 disubstituted piperidine with a sulfonamide group and (CH₂)₂OMe chain on the sulfonamide nitrogen. This study of the structure–activity relationships also showed that the absence of the *N*-alkyl chain on the carboxamide and

sulfonamide nitrogen is imperative for MAO-B inhibition, as compounds bearing the *N*-alkyl chain were inactive.

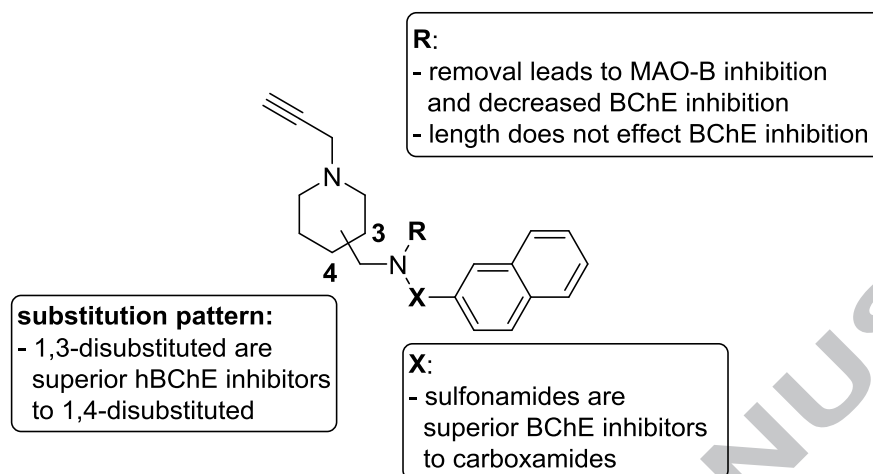


Figure 5. Structure–activity relationships of *N*-propargylpiperidines.

Crystal Structure of hBChE in Complex with Compound 3

The crystal structure of compound **3** in complex with hBChE was solved at 2.5 Å resolution, which revealed the molecular basis for the micromolar inhibitory potency of this *N*-propargylpiperidine. As expected, compound **3** shares a similar binding mode with the parent hit compound **1**, where the naphthalene moiety occupies the acyl-binding pocket and is T-stacked (i.e., π - π interaction) to Trp231 (Figure 6). Compared to the parent hit compound **1**, the positively charged nitrogen of the piperidine moiety does not interact with the Tyr332 side chain anymore, as the distance between the cation and the aromatic ring is too large (5.2 vs. 3.5 Å, to the closest aromatic carbon) [20]. These specificities appear to explain the difference in the inhibitory potencies between these two inhibitors (IC_{50} (**1**) = 21.3 nM; IC_{50} (**3**) = 3.306 μ M). In the complex structure, the (CH₂)₂OMe side-chain is oriented toward the choline-binding site and the catalytic His438, but this does not interact directly with any of the amino-

acid residues. Finally, the propargyl moiety lies over the backbone atoms of residues Asn68 to Asp70, and points out of the active site gorge.

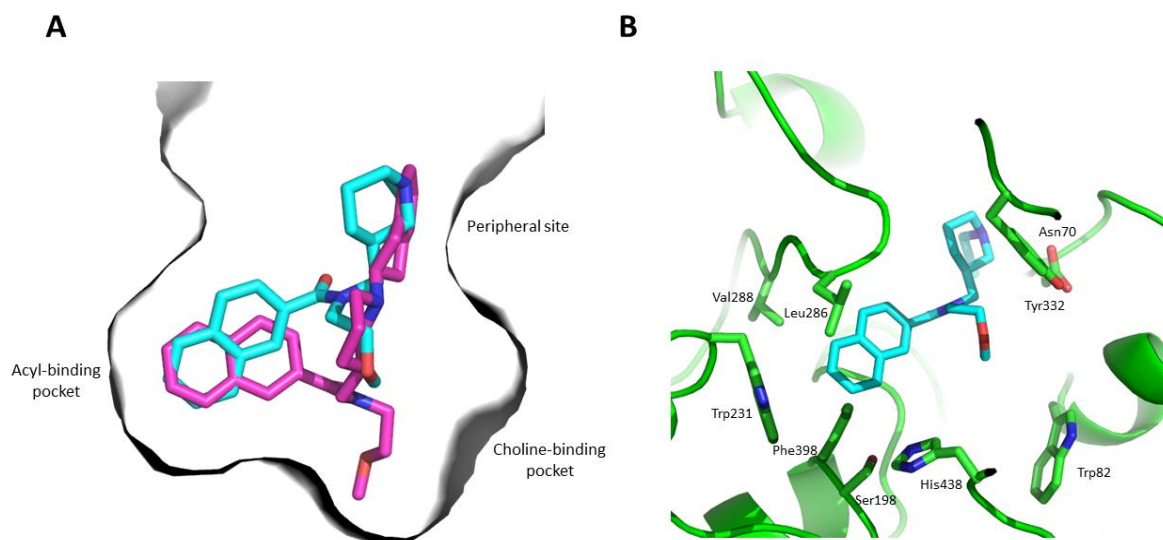


Figure 6. Crystal structure of compound **3** bound into the active site of hBChE (PDB code 5LKR). (A) Alignment of crystal structures of compound **3** (cyan) and hit compound **1** (purple) in their complexes with hBChE (gray surface). (B) Close-up view of compound **3** (cyan sticks) bound in the acyl-binding and choline-binding pockets and at the peripheral site of hBChE (green). Important active site residues are shown as sticks: catalytic residues (Ser198, His438); acyl-binding pocket residues (Trp231, Leu286, Val288, Phe398); choline-binding site (Trp82); and peripheral site (Asn70, Tyr332).

In-Vitro Blood-Brain Barrier Permeation of Compounds 3–7 and 32–38

As AD is a progressive brain disorder, drugs for its treatment should partition into the brain by crossing the blood-brain barrier (BBB). On this basis, the brain penetration of *N*-propargylpiperidines **4–8**, **14**, **15** and **22–25** were evaluated using the parallel artificial membrane permeation assay (PAMPA)–BBB method, which is a low cost and high-throughput assay that is used to exclude poorly permeable compounds from further testing (e.g., *in-vitro* assays on cell lines and *in-vivo* assays) [30]. Table 2 shows the logarithms of the

effective permeabilities ($\log P_e$) of the *N*-propargylpiperdines and eight reference drugs with known CNS penetration. For all of the *N*-propargylpiperdines, the $\log P_e$ values are higher than the limit of uncertain permeability (-5.0), which suggests that these should cross the BBB by passive diffusion.

Table 2. *In-vitro* blood-brain barrier permeation of *N*-propargyl piperidines and reference drugs.

Compound name or number	Log P_e^a	Permeability prediction
Verapamil HCl	-4.1	CNS+
Corticosterone	-5.0	CNS±
Progesterone	-4.0	CNS+
Lidocaine	-4.6	CNS+
Quinidine HCl	-4.3	CNS+
Theophylline	-6.9	CNS-
Propranolol HCl	-4.1	CNS+
Donepezil HCl	-4.0	CNS+
3	-4.3	CNS+
4	-4.0	CNS+
5	-4.1	CNS+
6	-4.0	CNS+
7	-4.0	CNS+
8	-3.9	CNS+
14	-4.0	CNS+
15	-4.3	CNS+
22	-4.4	CNS+
23	-4.5	CNS+
24	-3.9	CNS+
25	-3.9	CNS+

^a Data are means of two independent experiments

CNS+, $\log P_e > -5.0$, high permeability; CNS-, $\log P_e \leq -6.9$, low permeability; CNS±, $-6.9 < \log P_e \leq -5.0$, permeability uncertain

Inhibition of $A\beta_{1-42}$ Aggregation

Senile (amyloid) plaques that accumulate in the brains of patients with AD [31] are mainly composed of $A\beta_{1-42}$ [32]. This 42-amino-acid-long $A\beta$ isoform forms a variety of cytotoxic structures, which range from monomers to oligomers (i.e., 2-6 peptides) and fibers [1],[33]. The inhibitory activity of these *N*-propargylpiperidines against $A\beta_{1-42}$ aggregation was thus

evaluated with the thioflavine-T fluorometric assay [34]. Only compound **22** showed A β_{1-42} anti-aggregation effects, with modest 23.4% inhibition. Interestingly, replacement of the 1*H*-indene moiety of hit compound **1** (61.7% inhibition) [20] with the propargyl group (compound **3**, no inhibition) diminished the A β_{1-42} -anti-aggregation activity (Supplementary Table S1).

Cytotoxicity and Neuroprotective Effects of Compounds 6 and 7

Hit compound **1** and its most potent sulfonamide derivative (compound **2**) are non-cytotoxic to neuronal cells (SH-SY5Y) and can protect them from the toxic effects of A β_{1-42} [12],[20]. To determine whether *N*-propargyl derivatives share these non-cytotoxic and neuroprotective properties of the parent compounds, inhibitors **6** (dual hBChE and hMAO-B inhibitor) and **7** (most potent BChE inhibitor) were characterized accordingly.

First, their cytotoxicity profiles were determined using MTS (3-(4,5-dimethylthiazol-2-yl)-5-(3-carboxymethoxyphenyl)-2-(4-sulfophenyl)-2*H*-tetrazolium, inner salt) assay. At 5 μ M, compound **6** was completely non-cytotoxic and had an LD₅₀ of 241.8 μ M, a concentration 90-fold and 4-fold greater than those needed to achieve 50% inhibition of hBChE and MAO-B, respectively. At 2.5 μ M, compound **7** was completely non-cytotoxic and had an LD₅₀ of 48.13 μ M, a concentration 375-fold greater than that needed to achieve 50% inhibition of hBChE (Figure 7).

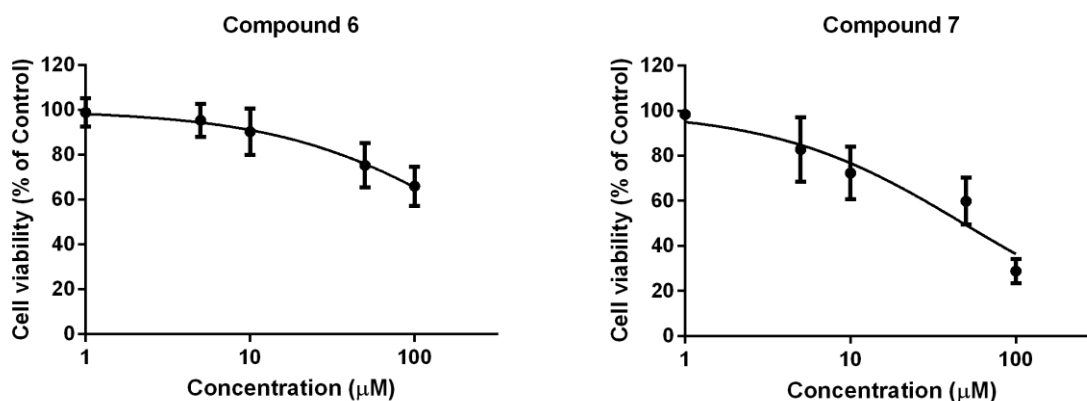


Figure 7. Concentration-dependent cytotoxicities of compounds **6** and **7**. SH-SY5Y cells were incubated in the presence of increasing concentrations of compounds **6** and **7** (1–100 μM). After 48 h, cell viability was evaluated using the MTS assay. The control group (DMSO) was considered as 100% cell viability. Cells were treated in quadruplicate. Data are means \pm SD of at least three independent experiments.

We then determined whether compounds **6** and **7** can protect neuronal cells from toxic $\text{A}\beta$ -species. Therefore, we examined neuronal death induced by $\text{A}\beta_{1-42}$ in the absence and presence of 5 μM compound **6** and 2.5 μM compound **7**. As shown in Figure 8, treatment of neuronal cells with 5 μM $\text{A}\beta_{1-42}$ caused significant toxicity, whereas compounds **6** and **7** prevented this $\text{A}\beta_{1-42}$ -induced cell death. These neuroprotective effects are independent of $\text{A}\beta_{1-42}$ aggregation, as at 10 μM , compounds **6** and **7** did not inhibit $\text{A}\beta_{1-42}$ aggregation in the Thioflavin-T (ThT) fluorometric assay (Supplementary Table S1).

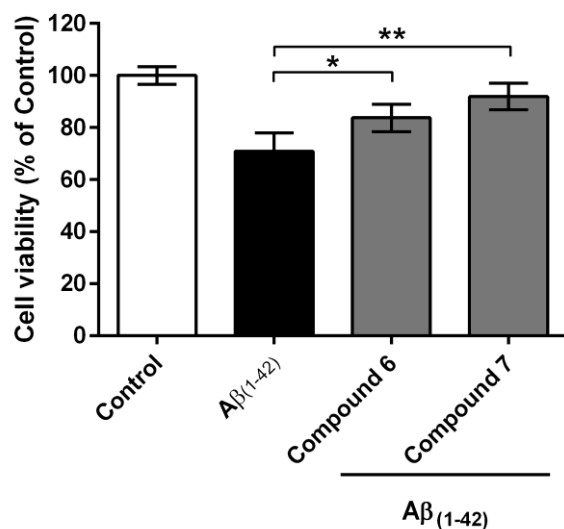


Figure 8. Neuroprotective effects of compounds **6** and **7** on A β_{1-42} -induced cytotoxicity in SH-SY5Y cells. Cells were treated with 5 μ M A β_{1-42} in the absence and presence of 5 μ M compound **6** and 2.5 μ M compound **7**. After 48 h the, neuroprotective effects were evaluated using the MTS assay. The control group (DMSO) was considered as 100% cell viability. Cells were treated in quadruplicate. Data are means \pm SD of three independent experiments. * P <0.01, ** P <0.05

CONCLUSIONS

We have here described the design, synthesis, and biochemical evaluation of 12 *N*-propargylpiperidines compounds. All of these compounds selectively inhibit hBChE over AChE, and the results from the PAMPA-BBB assay suggest that they should cross the BBB. The crystal structure of compound **3** in complex with hBChE revealed its mode of binding and also suggested ways to further optimize these *N*-propargylpiperidines. Three compounds also selectively inhibited MAO-B over MAO-A (i.e., **4**, **5**, **6**). One of these, the dual BChE and MAO-B inhibitor **6** ($IC_{50}(\text{hBChE}) = 2.6 \mu\text{M}$; $IC_{50}(\text{hMAO-B}) = 53.9 \mu\text{M}$), and the most potent hBChE inhibitor **7** ($IC_{50} = 0.127 \mu\text{M}$) were non-cytotoxic and protected neuronal cells from toxic A β_{1-42} . Compound **6** confirmed our hypothesis that replacing the *N*-piperidine

substituents of our neuroprotective selective hBChE inhibitors **1** and **2** with the propargyl moiety of selective irreversible propargylamine MAO-B inhibitors produces selective hBChE and MAO-B inhibitors with neuroprotective activity.

METHODS

General chemistry methods

^1H -NMR and ^{13}C -NMR were recorded at 400.130 MHz and 100.613 MHz, respectively, on an NMR spectrophotometer (Bruker Avance III). The chemical shifts (δ) are reported in parts per million (ppm) and are referenced to the deuterated solvent used. The coupling constants (J) are reported in Hz, and the splitting patterns are indicated as: s, singlet; bs, broad singlet; d, doublet; dd, doublet of doublets; td, triplet of doublets; h, hextet; m, multiplet; t, triplet; bt, broad triplet; dt, doublet of triplets; tt, triplet of triplets; q, quartet; qd, quartet of doublets. Infrared (IR) spectra were recorded on a FT-IR spectrometer (System Spectrum BX; Perkin-Elmer). ATR IR spectra were recorded on a FT-IR spectrometer (Thermo Nicolet Nexus 470 ESP). Mass spectra were recorded on a mass spectrometer (VG-Analytical AutoSpec Q Micromass). Melting points were determined on a Leica hot-stage microscope and are uncorrected. Evaporation of the solvents was performed under reduced pressure. Reagents and solvents were purchased from Acros Organics, Alfa Aesar, Euriso-Top, Fluka, Merck, Sigma-Aldrich, and TCI Europe, and were used without further purification, unless otherwise stated. Flash column chromatography was performed on silica gel 60 for column chromatography (particle size, 230-400 mesh). Analytical thin-layer chromatography was performed on silica gel aluminum sheets (0.20 mm; 60 F254; Merck), with visualization using ultraviolet light and/or visualization reagents. Analytical reversed-phase HPLC method A was performed on an LC system (Dionex Ultimate 3000 Binary Rapid Separation; Thermo Scientific) equipped with an autosampler, a binary pump system, a photodiode array detector, a thermostated

column compartment, and the Chromeleon Chromatography Data System. Analytical reversed-phase HPLC method B were performed on an LC modular system (Agilent 1100) equipped with an autosampler, a quaternary pump system, a photodiode array detector, a thermostated column compartment, a fraction collector compartment, and the ChemStation data system. The detector on both HPLC systems was set to 210 nm, 254 nm, and 280 nm. The column used for methods A and B was a C18 analytical column (150 × 4.6 mm, 5 μm; Zorbax Eclipse Plus; Agilent). An HPLC guard cartridge system was used (octadecyl; 4.0 × 3.0 mm ID; Security Guard Cartridge C18 CODS; Phenomenex). The HPLC columns were thermostated at 25 °C.

Method A: The sample solution (10 μL; 0.1 mg/mL in MeCN) was injected and eluted at a flow rate of 1 mL/min, using a linear gradient of mobile phase A (70% [v/v] 5 mM aqueous phosphate buffer, pH 8.00, in MeCN) and mobile phase B (30% [v/v] 5 mM aqueous phosphate buffer, pH 8.00, in MeCN). The gradient for method A (for mobile phase B) was: 0–7 min, 0%–100%; 7–20 min, 100%.

Method B: The sample solution (10 μL; 0.1 mg/mL in MeCN) was injected and eluted at a flow rate of 1 mL/min, using a linear gradient of mobile phase A (70% [v/v] 5 mM aqueous phosphate buffer, pH 8.00, in MeCN) and mobile phase B (30% [v/v] 5 mM aqueous phosphate buffer, pH 8.00, in MeCN). The gradient for method A (for mobile phase B) was: 0–7 min, 0%–100%; 7–15 min, 100%, 15–20 min, 100%–0%.

General synthetic procedures

General procedure for debenzoylation (general procedure 1)

The benzyl amine (1.0 equiv.) was dissolved in MeOH at room temperature. The solution was stirred and agitated with a stream of argon for 30 min. Pd(OH)₂ on carbon (20 wt.%) (20% mass of benzyl amine) was added, followed by cyclohexene (10.0 equiv.). The resulting suspension was refluxed under an atmosphere of argon for 20 h, then filtered under suction through a pad of Celite, and evaporated to produce the crude secondary amine, which was used in the next step without further purification.

General procedure for alkylation of piperidine nitrogen with propargly bromide (general procedure 2)

Piperidine (1.0 equiv.) was dissolved in acetone at room temperature. The solution was stirred and Cs₂CO₃ (1.0 equiv.) was added, followed by propargly bromide (80 wt. % solution in toluene, 1.0 equiv.). The reaction mixture was protected from the light by wrapping the flask with aluminum foil. After 24 h, the reaction mixture was evaporated, and EtOAc (60 mL) was added to the residue. The suspension was transferred into a separating funnel and extracted with water (60 mL) followed by saturated aqueous NaHCO₃ solution (60 mL), dried over anhydrous Na₂SO₄, and evaporated. The crude product was purified by flash column chromatography.

General procedure for removal of Boc-protective group with 2 M HCl solution in Et₂O (general procedure 3)

The amine (1.0 equiv.) was dissolved in MeOH at room temperature. The solution was stirred and agitated with a stream of argon for 15 min, and then cooled to 0 °C. A solution 2 M HCl in Et₂O (10 equiv.) was added drop-wise, then allowed to warm to room temperature, and stirred for 24 h. The reaction mixture was evaporated, and Et₂O (50 mL) was added to the oily residue obtained. The flask was placed in an ultrasonic bath for 15 min. During this time, the

oily residue transformed into a solid. The flask was removed from the ultrasonic bath and the precipitate was allowed to settle to the bottom of the flask. The supernatant was removed, Et₂O (50 mL) was added, and the flask was placed back in the ultrasonic bath for 1 min. The flask was removed from the ultrasonic bath and the precipitate was allowed to settle to the bottom of the flask. The supernatant was removed, Et₂O (50 mL) was added again, and this procedure was repeated two more times. After the final supernatant was removed, the solid residue was dried at reduced pressure. The crude product was used in the next step without further purification.

General procedure for removal of Boc-protective group with TFA (general procedure 4)

The amine (1.0 equiv.) was dissolved in DCM at room temperature. The solution was stirred and TFA (20.0 equiv.) was added drop-wise. After 24 h, the reaction mixture was evaporated and Et₂O (50 mL) was added to the oily residue. The flask was placed in an ultrasonic bath for 15 min. During this time, the oily residue transformed into a solid. The flask was removed from the ultrasonic bath, and the precipitate was allowed to settle to the bottom of the flask. The supernatant was removed, Et₂O (50 mL) was added, and the flask was placed back in the ultrasonic bath for 1 min. The flask was removed from the ultrasonic bath, and the precipitate was allowed to settle to the bottom of the flask. The supernatant was removed, Et₂O (50 mL) was added again, and this procedure was repeated two more times. After the final supernatant was removed, the solid residue was dried at reduced pressure. The crude product was used in the next step without further purification.

General procedure for formation of carboxamide bond (general procedure 4) and sulfonamide bond (general procedure 5)

The salt of the amine (1.0 equiv.) was dissolved in DCM and cooled to 0 °C. The reaction mixture was stirred and trimethylamine (Et₃N; 3.0 equiv.) was added drop-wise. After 15 min, 2-naphthoyl chloride (1.0 equiv.) or naphthalene-2-sulfonyl chloride (1.0 equiv.) was added, and the reaction mixture was allowed to warm up to room temperature, and then stirred for 24 h. The reaction mixture was transferred into a separating funnel, washed with water, followed by saturated aqueous NaHCO₃ solution, dried over anhydrous Na₂SO₄, and evaporated. The crude product was purified by flash column chromatography.

All of the final compounds were appropriately characterized and were of high purity (>95%; analytical HPLC, Supplementary Information).

Characterization of the final compounds

(±)-*N*-((1-(prop-2-ynyl)piperidin-3-yl)methyl)-2-naphthamide (4)

R_f = 0.49 (DCM/MeOH, 10:1, v/v). mp 112–115 °C. IR (ATR): 3304, 3270, 2929, 2789, 1625, 1534, 1309, 1242, 1115, 897, 779, 734, 689 cm⁻¹. ¹H-NMR (400.130 MHz, CDCl₃): δ = 1.12–1.21 (1 H, m), 1.59–1.69 (1 H, m), 1.80 (2 H, d, J = 10.0 Hz), 2.04 (1 H, bs), 2.19–2.37 (3 H, m), 2.79 (1 H, d, J = 10.4 Hz), 2.91 (1 H, d, J = 10.9 Hz), 3.35 (2 H, d, J = 2.1 Hz), 3.47 (2 H, t, J = 6.3 Hz), 6.73 (1 H, bs), 7.51–7.58 (2 H, m), 7.82–7.92 (4 H, m), 8.29 (1 H, s). ¹³C-NMR (100.613 MHz, CDCl₃): δ = 24.43 (CH₂), 28.00 (CH), 36.24 (CH₂), 43.78 (CH₂), 47.23 (CH₂), 52.57 (CH₂), 56.42 (CH₂), 73.12 (CH), 78.81 (C), 123.56 (CH), 126.47 (CH), 127.21 (CH), 127.35 (CH), 127.52 (CH), 128.15 (CH), 128.71 (CH), 131.78 (C), 132.40 (C), 134.44 (C), 167.61 (CO). HRMS (ESI⁺): m/z calcd for C₂₀H₂₃N₂O 307.1810; found 307.1811. HPLC purity, 99% at 254 nm (method B, t_R = 8.27 min).

(±)-*N*-(2-methoxyethyl)-*N*-((1-(prop-2-ynyl)piperidin-3-yl)methyl)-2-naphthamide (3)

$R_f = 0.43$ (DCM/MeOH, 10:1, v/v). IR (ATR): 3235, 2929, 2808, 1622, 1476, 1421, 1288, 1194, 1115, 1071, 900, 823, 757 cm^{-1} . $^1\text{H-NMR}$ (400.130 MHz, CDCl_3): $\delta = 0.83$ (1 H, dd, $J_1 = 217.1$ Hz, $J_2 = 7.0$ Hz), 1.47–2.93 (9 H, m), 3.18–3.54 (7 H, m), 3.51 (2 H, d, $J = 28.2$ Hz), 3.69–3.78 (2 H, m), 7.43–7.49 (3 H, m), 7.80–7.84 (4 H, m). $^{13}\text{C-NMR}$ (100.613 MHz, CDCl_3): $\delta = 24.49$ (CH_2), 24.68 (CH_2), 27.57 (CH), 27.93 (CH), 35.00 (CH_2), 35.12 (CH_2), 44.75 (CH_2), 47.07 (CH_2), 47.26 (CH_2), 47.56 (CH_2), 48.03 (CH_2), 48.66 (CH_2), 52.18 (CH_2), 52.70 (CH_2), 53.80 (CH_2), 55.78 (CH_2), 56.47 (CH_2), 58.70 (CH_3), 70.21 (CH_2), 70.44 (CH_2), 73.10 (CH), 78.39 (C), 78.86 (C), 124.18 (CH), 126.12 (CH), 126.23 (CH), 126.39 (CH), 126.65 (CH), 127.59 (CH), 128.08 (CH), 128.12 (CH), 132.48 (C), 133.16 (C), 134.02 (C), 172.08 (CO), 172.33 (CO) [35]. HRMS (ESI+): m/z calcd for $\text{C}_{23}\text{H}_{29}\text{N}_2\text{O}_2$ 365.2229; found 365.2221. HPLC purity, 98% at 254 nm (method B, $t_R = 9.11$ min).

(±)-*N*-(3-methoxypropyl)-*N*-((1-(prop-2-ynyl)piperidin-3-yl)methyl)-2-naphthamide (15)

$R_f = 0.45$ (DCM/MeOH, 10:1, v/v). IR (ATR): 3228, 2929, 2805, 1622, 1476, 1423, 1301, 1197, 1114, 900, 864, 756 cm^{-1} . $^1\text{H-NMR}$ (400.130 MHz, CDCl_3): $\delta = 0.84$ (1 H, dd, $J_1 = 214.6$ Hz, $J_2 = 8.3$ Hz), 1.44–2.26 (9 H, m), 2.65–2.75 (1 H, m), 2.87 (1 H, dd, $J_1 = 35.6$ Hz, $J_2 = 7.8$ Hz), 3.09–3.38 (8 H, m), 3.49 (2 H, bs), 3.57–3.66 (1 H, m), 7.42 (1 H, d, $J = 7.8$ Hz), 7.46–7.50 (2 H, m), 7.80–7.86 (4 H, m). $^{13}\text{C-NMR}$ (100.613 MHz, CDCl_3): $\delta = 24.51$ (CH_2), 24.73 (CH_2), 27.38 (CH), 27.62 (CH), 28.04 (CH_2), 28.52 (CH_2), 34.91 (CH_2), 35.15 (CH_2), 42.46 (CH_2), 46.36 (CH_2), 47.10 (CH_2), 47.30 (CH_2), 47.44 (CH_2), 52.20 (CH_2), 52.25 (CH_2), 52.77 (CH_2), 53.00 (CH_2), 55.84 (CH_2), 56.50 (CH_2), 58.27 (CH_3), 58.51 (CH_3), 69.15 (CH_2), 70.23 (CH_2), 73.12 (CH), 78.40 (C), 78.85 (C), 123.87 (CH), 124.19 (CH), 125.86 (CH), 126.24 (CH), 126.42 (CH), 126.66 (CH), 127.62 (CH), 128.11 (CH), 132.53 (C), 133.21 (C),

134.13 (C), 171.98 (C), 172.09 (C) [35]. HRMS (ESI+): m/z calcd for $C_{24}H_{31}N_2O_2$ 379.2386; found 379.2376. HPLC purity, 97% at 254 nm (method B, t_R = 9.31 min).

N-((1-(prop-2-ynyl)piperidin-4-yl)methyl)-2-naphthamide (5)

R_f = 0.41 (DCM/MeOH, 10:1, v/v). IR (ATR): 3298, 3264, 2922, 2837, 1638, 1542, 1428, 1300, 1147, 1108, 895, 740, 690 cm^{-1} . 1H -NMR (400.130 MHz, $CDCl_3$): δ = 1.59 (2 H, bs), 1.81 (1 H, bs), 1.90 (2 H, d, J = 12.7 Hz), 2.34 (1 H, s), 2.45 (2 H, bs), 3.05 (2 H, bs), 3.44 (4 H, t, J = 6.2 Hz), 6.52 (1 H, bs), 7.52–7.59 (2 H, m), 7.82–7.94 (4 H, m), 8.30 (1 H, s). ^{13}C -NMR (100.613 MHz, $CDCl_3$): δ = 29.77 (CH_2), 35.44 (CH), 45.35 (CH_2), 46.92 (CH_2), 51.86 (CH_2), 72.91 (CH), 78.82 (C), 123.52 (CH), 126.45 (CH), 127.15 (CH), 127.32 (CH), 127.49 (CH), 128.12 (CH), 128.64 (CH), 131.76 (C), 132.38 (C), 134.44 (C), 167.71 (C). HRMS (ESI+): m/z calcd for $C_{20}H_{23}N_2O$ 307.1810; found 307.1805. HPLC purity, 98% at 254 nm (method B, t_R = 8.08 min).

N-(2-methoxyethyl)-N-((1-(prop-2-ynyl)piperidin-4-yl)methyl)-2-naphthamide (22)

R_f = 0.44 (DCM/MeOH, 10:1, v/v). IR (ATR): 3228, 2924, 1622, 1476, 1422, 1285, 1115, 1070, 976, 899, 823, 757 cm^{-1} . 1H -NMR (400.130 MHz, $CDCl_3$): δ = 0.94–1.03 (1 H, m), 1.51–1.98 (4 H, m), 2.07–2.40 (3 H, m), 2.78 (1 H, d, J = 7.9 Hz), 3.00 (1 H, bs), 3.22–3.42 (7 H, m), 3.50 (2 H, bs), 3.73 (2 H, m), 7.42–7.55 (3 H, m), 7.83–7.86 (4 H, m). ^{13}C -NMR (100.613 MHz, $CDCl_3$): δ = 29.31 (CH_2), 29.87 (CH_2), 33.86 (CH), 44.65 (CH_2), 46.76 (CH_2), 46.90 (CH_2), 49.43 (CH_2), 50.69 (CH_2), 51.63 (CH_2), 51.90 (CH_2), 55.45 (CH_2), 58.71 (CH_3), 70.28 (CH_2), 70.53 (CH_2), 72.92 (CH), 78.58 (C), 78.70 (C), 124.17 (CH), 126.23 (CH), 126.40 (CH), 126.67 (CH), 127.57 (CH), 128.07 (CH), 128.09 (CH), 132.45 (CH), 133.16 (C), 133.83 (C), 134.10 (C), 172.23 (C), 172.32 (C) [35]. HRMS (ESI+): m/z calcd for

C₂₃H₂₉N₂O₂ 365.2229; found 365.2231. HPLC purity, 98% at 254 nm (method B, t_R = 8.86 min).

***N*-(3-methoxypropyl)-*N*-((1-(prop-2-ynyl)piperidin-4-yl)methyl)-2-naphthamide (23)**

R_f = 0.45 (DCM/MeOH, 10:1, v/v). IR (ATR): 3226, 2923, 1621, 1423, 1477, 1300, 1228, 1113, 898, 823, 756 cm⁻¹. ¹H-NMR (400.130 MHz, CDCl₃): δ = 0.93–1.04 (1 H, m), 1.51–2.02 (6 H, m), 2.08–2.39 (3 H, m), 2.78 (1 H, d, J = 8.9 Hz), 2.99 (1 H, d, J = 8.0 Hz), 3.13–3.46 (9 H, m), 3.52–3.55 (1 H, m), 3.61–3.66 (1 H, m), 7.43 (1 H, q, J = 8.3 Hz), 7.49–7.54 (2 H, m), 7.80–7.85 (4 H, m). ¹³C-NMR (100.613 MHz, CDCl₃): δ = 27.44 (CH₂), 28.67 (CH₂), 29.34 (CH₂), 29.91 (CH₂), 33.68 (CH), 33.88 (CH), 42.29 (CH₂), 46.75 (CH₂), 46.91 (CH₂), 47.16 (CH₂), 50.14 (CH₂), 51.57 (CH₂), 51.86 (CH₂), 54.66 (CH₂), 58.22 (CH₃), 58.50 (CH₃), 69.09 (CH₂), 70.23 (CH₂), 72.94 (CH), 78.54 (C), 78.68 (C), 123.89 (CH), 124.11 (CH), 125.85 (CH), 126.21 (CH), 126.40 (CH), 126.65 (CH), 127.57 (CH), 128.08 (CH), 132.47 (CH), 133.15 (C), 133.98 (C), 134.09 (C), 172.04 (C) [35]. HRMS (ESI⁺): m/z calcd for C₂₄H₃₁N₂O₂ 379.2386; found 379.2383. HPLC purity, 97% at 254 nm (method B, t_R = 9.07 min).

(±)-*N*-((1-(prop-2-ynyl)piperidin-3-yl)methyl)naphthalene-2-sulfonamide (8)

R_f = 0.44 (DCM/MeOH, 10:1, v/v). mp 133–136 °C. IR (ATR): 3247, 3050, 2934, 2808, 2688, 1307, 1147, 1081, 821, 756, 655, 615 cm⁻¹. ¹H-NMR (400.130 MHz, CDCl₃): δ = 0.97–1.05 (1 H, m), 1.59–1.77 (3 H, m), 1.87–1.93 (1 H, m), 2.06–2.12 (1 H, m), 2.25–2.34 (2 H, m), 2.78–2.81 (1 H, m), 2.86–2.97 (3 H, m), 3.34 (2 H, d, J = 2.0 Hz), 5.23 (1 H, bs), 7.59–7.67 (2 H, m), 7.84 (1 H, dd, J_1 = 8.7 Hz, J_2 = 1.8 Hz), 7.90–7.92 (1 H, m), 7.97 (2 H, d, J = 8.9 Hz), 8.43 (1 H, d, J = 1.1 Hz). ¹³C-NMR (100.613 MHz, CDCl₃): δ = 23.75 (CH₂), 27.28 (CH), 35.60 (CH₂), 46.71 (CH₂), 47.06 (CH₂), 52.38 (CH₂), 55.64 (CH₂), 74.57 (CH), 77.20

(C), 122.28 (CH), 127.53 (CH), 127.90 (CH), 128.37 (CH), 128.74 (CH), 129.22 (CH), 129.54 (CH), 132.11 (C), 134.77 (C), 136.56 (C). HRMS (ESI+): m/z calcd for C₁₉H₂₃N₂O₂S 343.1480; found 343.1485. HPLC purity, 96% at 254 nm (method A, t_R = 7.14 min).

(±)-N-(2-methoxyethyl)-N-((1-(prop-2-ynyl)piperidin-3-yl)methyl)naphthalene-2-sulfonamide (14)

R_f = 0.50 (DCM/MeOH, 10:1, v/v). IR (ATR): 3275, 3056, 2928, 2805, 1330, 1154, 1114, 1073, 860, 817, 750, 649, 614 cm⁻¹. ¹H-NMR (400.130 MHz, CDCl₃): δ = 0.92–1.02 (1 H, m), 1.58–1.67 (1 H, m), 1.71–1.78 (2 H, m), 1.95–2.10 (2 H, m), 2.23 (2 H, s), 2.83–2.90 (2 H, m), 3.09–3.20 (2 H, m), 3.23 (3 H, s), 3.28–3.36 (4 H, m), 3.48–3.53 (2 H, m), 7.58–7.66 (2 H, m), 7.78 (1 H, dd, J_1 = 8.7 Hz, J_2 = 1.8 Hz), 7.89–7.92 (1 H, m), 7.94–7.98 (2 H, m), 8.38–8.39 (1 H, m). ¹³C-NMR (100.613 MHz, CDCl₃): δ = 24.50 (CH₂), 27.76 (CH), 34.86 (CH₂), 47.16 (CH₂), 48.00 (CH₂), 52.53 (CH₂), 53.08 (CH₂), 56.20 (CH₂), 58.56 (CH₃), 71.00 (CH₂), 73.08 (CH), 78.66 (C), 122.41 (CH), 127.33 (CH), 127.70 (CH), 128.26 (CH), 128.50 (CH), 129.01 (CH), 129.10 (CH), 131.97 (C), 134.51 (C), 136.28 (C). HRMS (ESI+): m/z calcd for C₂₂H₂₉N₂O₃S 401.1899; found 401.1890. HPLC purity, 96% at 254 nm (method A, t_R = 8.59 min).

(±)-N-(3-methoxypropyl)-N-((1-(prop-2-ynyl)piperidin-3-yl)methyl)naphthalene-2-sulfonamide (7)

R_f = 0.52 (DCM/MeOH, 10:1, v/v). IR (ATR): 3274, 3056, 2929, 2806, 1332, 1154, 1113, 1073, 861, 88, 749, 650, 615 cm⁻¹. ¹H-NMR (400.130 MHz, CDCl₃): δ = 0.92–1.03 (1 H, m), 1.55–1.66 (1 H, m), 1.72–1.84 (4 H, m), 1.94–2.03 (2 H, m), 2.22 (2 H, s), 2.81–2.87 (2 H, m), 3.02–3.16 (2 H, m), 3.23–3.36 (9 H, m), 7.58–7.66 (2 H, m), 7.77 (1 H, dd, J_1 = 8.5 Hz, J_2 = 1.9 Hz), 7.89–7.98 (3 H, m), 8.37–8.38 (1 H, m). ¹³C-NMR (100.613 MHz, CDCl₃): δ =

24.37 (CH₂), 27.74 (CH), 28.74 (CH₂), 34.68 (CH₂), 46.05 (CH₂), 47.04 (CH₂), 52.26, 52.43 (CH₂), 56.15 (CH₂), 58.28 (CH₃), 69.52 (CH₂), 73.02 (CH), 78.58 (C), 122.26 (CH), 127.23 (CH), 127.60 (CH), 128.10 (CH), 128.38 (CH), 128.90 (CH), 129.08 (CH), 131.88 (C), 134.38 (C), 136.17 (C). HRMS (ESI⁺): *m/z* calcd for C₂₃H₃₁N₂O₃S 415.2055; found 415.2052. HPLC purity, 97% at 254 nm (method A, *t_R* = 8.86 min).

N-((1-(prop-2-ynyl)piperidin-4-yl)methyl)naphthalene-2-sulfonamide (6)

R_f = 0.51 (DCM/MeOH, 10:1, v/v). mp 111–114 °C. IR (ATR): 3266, 3052, 2912, 2780, 2749, 1312, 1063, 868, 828, 740, 628 cm⁻¹. ¹H-NMR (400.130 MHz, CDCl₃): δ = 1.20–1.30 (2 H, m), 1.43–1.54 (1 H, m), 1.72 (2 H, d, *J* = 13.6 Hz), 2.17 (2 H, t, *J* = 11.1 Hz), 2.23 (1 H, t, *J* = 2.4 Hz), 2.83–2.88 (4 H, m), 3.29 (2 H, d, *J* = 2.4 Hz), 4.95 (1 H, t, *J* = 6.2 Hz), 7.59–7.67 (2 H, m), 7.84 (1 H, dd, *J*₁ = 8.7 Hz, *J*₂ = 1.8 Hz), 7.90–7.92 (1 H, m), 7.95–7.97 (2 H, m), 8.43–8.44 (1 H, m). ¹³C-NMR (100.613 MHz, CDCl₃): δ = 29.34 (CH₂), 35.36 (CH), 46.76 (CH₂), 48.37 (CH₂), 51.60 (CH₂), 72.99 (CH), 78.68 (C), 122.05 (CH), 127.30 (CH), 127.65 (CH), 128.07 (CH), 128.50 (CH), 128.96 (CH), 129.29 (CH), 131.85 (C), 134.46 (C), 136.53 (C). HRMS (ESI⁺): *m/z* calcd for C₁₉H₂₃N₂O₂S 343.1480; found 343.1477. HPLC purity, 97% at 254 nm (method A, *t_R* = 6.69 min).

N-(2-methoxyethyl)-N-((1-(prop-2-ynyl)piperidin-4-yl)methyl)naphthalene-2-sulfonamide (24)

R_f = 0.55 (DCM/MeOH, 10:1, v/v). mp 36–39 °C. IR (ATR): 3276, 3056, 2919, 2807, 2757, 1331, 1151, 1115, 988, 750, 649 cm⁻¹. ¹H-NMR (400.130 MHz, CDCl₃): δ = 1.25–1.34 (2 H, m), 1.66–1.78 (3 H, m), 2.21–2.26 (3 H, m), 2.91 (2 H, d, *J* = 11.5 Hz), 3.10 (2 H, d, *J* = 7.2 Hz), 3.24 (3 H, s), 3.29–3.36 (4 H, m), 3.50 (2 H, t, *J* = 5.9 Hz), 7.58–7.66 (2 H, m), 7.78 (1 H, dd, *J*₁ = 8.7 Hz, *J*₂ = 1.9 Hz), 7.89–7.97 (3 H, m), 8.38–8.39 (1 H, m). ¹³C-NMR (100.613

MHz, CDCl₃): δ = 29.59 (CH₂), 34.21 (CH), 46.83 (CH₂), 48.30 (CH₂), 51.79 (CH₂), 55.00 (CH₂), 58.52 (CH₃), 71.15 (CH₂), 73.00 (CH), 78.72 (C), 122.36 (CH), 127.31 (CH), 127.66 (CH), 128.24 (CH), 128.49 (CH), 128.96 (CH), 129.07 (CH), 131.91 (C), 134.46 (C), 136.16 (C). HRMS (ESI+): m/z calcd for C₂₂H₂₉N₂O₃S 401.1899; found 401.1891. HPLC purity, 98% at 254 nm (method A, t_R = 8.23 min).

***N*-(3-methoxypropyl)-*N*-((1-(prop-2-ynyl)piperidin-4-yl)methyl)naphthalene-2-sulfonamide (25)**

R_f = 0.69 (DCM/MeOH, 10:1, v/v). mp 80–83 °C. IR (ATR): 3275, 2984, 2924, 2809, 2764, 1332, 1108, 990, 765, 650 cm⁻¹. ¹H-NMR (400.130 MHz, CDCl₃): δ = 1.25–1.35 (2 H, m), 1.63–1.72 (1 H, m), 1.75–1.84 (4 H, m), 2.22–2.27 (3 H, m), 2.90 (2 H, d, J = 11.5 Hz), 3.04 (2 H, d, J = 7.3 Hz), 3.22–3.26 (5 H, m), 3.31–3.37 (4 H, m), 7.58–7.66 (2 H, m), 7.77 (1 H, dd, J_1 = 8.7 Hz, J_2 = 1.9 Hz), 7.89–7.98 (3 H, m), 8.37–8.38 (1 H, m). ¹³C-NMR (100.613 MHz, CDCl₃): δ = 28.99 (CH₂), 29.79 (CH₂), 34.29 (CH), 46.47 (CH₂), 46.89 (CH₂), 51.77 (CH₂), 54.46 (CH₂), 58.45 (CH₃), 69.64 (CH₂), 73.00 (CH), 78.75 (C), 122.41 (CH), 127.34 (CH), 127.70 (CH), 128.28 (CH), 128.49 (CH), 129.01 (CH), 129.15 (CH), 131.98 (C), 134.49 (C), 136.20 (C). HRMS (ESI+): m/z calcd for C₂₃H₃₁N₂O₃S 415.2055; found 415.2052. HPLC purity, 96% at 254 nm (method A, t_R = 8.46 min).

***In-Vitro* Enzyme Inhibition Assays**

ChE Inhibition Assay

The inhibitory potencies of the compounds against the ChEs were determined using the method of Ellman [28]. 5,5'-Dithiobis (2-nitrobenzoic acid) (Ellman's reagent; DTNB), and the butyrylthiocholine and acetylthiocholine iodides were from Sigma-Aldrich (Steinheim, Germany). mAChE and recombinant hBChE at the stock concentration of 4.6 mg mL⁻¹ in 10

mM MES buffer (pH 6.5) were kindly donated by Florian Nachon (IBS, Grenoble). The enzyme solutions were prepared by dilution of the concentrated stocks in 0.1 M phosphate-buffered solution, pH 8.0. The reactions were carried out in a final volume of 300 μ L of 0.1 M phosphate-buffered solution, pH 8.0, containing 333 μ M DTNB, 5×10^{-4} M butyrylthiocholine/ acetylthiocholine and 1×10^{-9} M or 5×10^{-11} M hBChE or mAChE, respectively. The reactions were started by addition of the substrate, at room temperature. The final content of the organic solvent (DMSO) was always 1%. The formation of the yellow 5-thio-2-nitrobenzoate anion as a result of the reaction of DTNB with the thiocholines was monitored for 1 min, as the change in absorbance at 412 nm, using a 96-well microplate reader (Synergy™ H4; BioTek Instruments, Inc., USA). To determine the blank value (b), phosphate-buffered solution replaced the enzyme solution. The initial velocity (v_0) was calculated from the slope of the linear trend obtained, with each measurement carried out in triplicate. For the first inhibitory screening, stock solutions of the test compounds (1 mM) were prepared in DMSO. The compounds were added to each well at a final concentration of 10 μ M. The reactions were started by addition of the substrate to the enzyme and inhibitor that had been preincubated for 5 min, to allow complete equilibration of the enzyme–inhibitor complexes. The initial velocities in the presence of the test compounds (v_i) were calculated. The inhibitory potencies are expressed as the residual activities ($RA = (v_i - b) / (v_0 - b)$). For the IC_{50} measurements, eight different concentrations of each compound were used to obtain enzyme activities of between 5% and 90%. The IC_{50} values were obtained by plotting the residual enzyme activities against the applied inhibitor concentrations, with the experimental data fitted to Equation (1):

$$Y = \text{Bottom} + (\text{Top} - \text{Bottom}) / (1 + 10^{((\text{Log}IC_{50} - X) \times \text{HillSlope}))} \quad (1),$$

where X is the logarithm of the inhibitor concentration, and Y is the residual activity. For the fitting procedure, the Gnuplot software and an in-house python script were used.

MAO Inhibition Assay

The effects of the test compounds on hMAO-A and hMAO-B were investigated using a fluorimetric assay, following a previously described literature method, with minor modifications [17]. The inhibitory activity of the compounds was evaluated by their effects on the production of hydrogen peroxide (H_2O_2) from *p*-tyramine, which was used as a nonspecific substrate for both of these hMAO isoforms. The production of the H_2O_2 was detected using Amplex Red reagent in the presence of horseradish peroxidase, where a highly sensitive fluorescent product, resorufin, is produced at stoichiometric amounts. Recombinant human microsomal hMAO enzymes expressed in baculovirus infected insect cells (BTI-TN-5B1-4), horse-radish peroxidase (type II, lyophilized powder), and *p*-tyramine hydrochloride were obtained from Sigma Aldrich. 10-Acetyl-3,7-dihydroxyphenoxazine (Amplex Red reagent) was synthesized as described in the literature [36].

Briefly, 100 μ L 50 mM sodium phosphate buffer (pH 7.4, 0.05% [v/v] Triton X-114) containing the compounds or the reference inhibitors and hMAO-A or hMAO-B required to oxidise (in the control group) approximately 15 pmol of *p*-tyramine/min (hMAO-A, 0.25 μ g protein; hMAO-B, 1.2 μ g protein) were incubated for 15 min at 37 °C in a flat-bottomed black 96-well microplate (μ CLEAR® microplate; Greiner Bio One International GmbH, Germany), and placed in a dark microplate reader chamber. After the pre-incubation, the reaction was started by adding the final concentrations of 250 μ M Amplex Red reagent, 4 U/mL horseradish peroxidase, and 1 mM *p*-tyramine (final volume, 200 μ L). The production of resorufin was quantified on the basis of the fluorescence generated ($\lambda_{ex} = 530$ nm, $\lambda_{em} = 590$ nm) at 37 °C over a period of 20 min, during which time the fluorescence increase linearly.

For control experiments, DMSO was used instead of the appropriate dilutions of the compounds in DMSO. To determine the blank value (b), phosphate-buffered solution replaced the enzyme solution. The initial velocities were calculated from the trends obtained, with each measurement carried out in duplicate. The specific fluorescence emission to obtain the final results was calculated after subtraction of the blank activity (b). The inhibitory potencies are expressed as the residual activities ($RA = (v_i - b) / (v_o - b)$), where v_i is the velocity in the presence of the test compounds, and v_o the control velocity in the presence of DMSO. The IC_{50} values were obtained by plotting residual enzyme activities against applied inhibitor concentration, with the experimental data fitted to a Hill four parameter equation (Equation (1)) using in-house python script and Gnuplot software. The capacity of the test compounds to react directly with Amplex Red was determined by adding these compounds to a solution containing all of the components except the MAO isoenzyme. No significant interference was detected for the test compounds.

For the reversibility assay, hMAO-B at 100-fold final concentration was incubated with the inhibitors at a concentration 10-fold the IC_{50} at 37 °C (volume, 50 μ L). After 15 min, the mixture was diluted 100-fold into the reaction buffer containing Amplex Red reagent, horseradish peroxidase, and *p*-tyramine hydrochloride. The final concentrations of all of the reagents and MAO-B were the same as in the assay described above. The reaction was monitored for 30 min. Control experiments were carried out in the same manner, where the inhibitor solution was replaced by DMSO.

Crystallization, Data Collection, and Processing

hBChE from insect cells was concentrated to 5.5 mg mL⁻¹ in 20 mM Tris, pH 7.4, and crystallized as previously described [37]. Briefly, crystals were grown at room temperature using the hanging-drop vapor diffusion method. The mother liquor solution was composed of

0.2 M ammonium acetate, 18% polyethylene glycol 4000. Crystals were soaked for 4 h in a solution of the mother liquor complemented with racemic compound **3** at 100 μ M. Prior to data collection, the crystals were cryoprotected by a short soak in mother liquor solution complemented with 18% glycerol, before being flash-cooled at 100K in liquid nitrogen. Data were collected at the automated beamline ID30A1 of the European Synchrotron Radiation Facility (Grenoble, France), using a wavelength of 0.966 Å. Data were indexed and integrated using XDS [38], and were scaled and merged with XSCALE and XDSCONV. The structure was solved using the molecular replacement method, using PHASER [39]. The search model was the hBChE model (PDB code 4TPK), from which all of the ligands and sugars were removed. Reciprocal-space refinement was performed using Phenix [40]. Following an initial rigid-body refinement, cycles of energy minimization, and individual isotropic temperature factor refinement were performed. Between cycles of model refinement, Coot [41] was used to conduct sessions of model rebuilding [41]. The ligand topology was generated using the PRODRG server [42]. Two ligands have been fitted in the active site of the two monomers present in the asymmetric unit. However, not all atoms of ligand bound to monomer A have been modeled. Indeed, only atoms of the naphthalene moiety could be fitted in the electron density. In monomer B, all atoms have been placed. Occupancies of the ligands have been refined. The coordinates and structure factors have been deposited in the Protein Data Bank under accession code 5LKR.

***In-Vitro* Blood–Brain Barrier Permeation Assay**

To estimate the potential of compounds **4–8**, **14**, **15** and **22–25** to cross the blood–brain barrier (BBB), the parallel artificial membrane permeability assay for BBB (PAMPA-BBB) was performed. The PAMPA-BBB Explorer Test System was obtained from pION (pION Inc., MA, USA). The assay was carried out following the pION standard procedure for BBB

permeability determination. Briefly, the test compounds and a set of seven standard compounds plus donepezil hydrochloride were dissolved in DMSO at 10 mM (or 50 mM for lidocaine and theophylline). The stock DMSO solutions were further diluted in Prisma HT buffer, pH 7.40 (5 μ L to 1 mL). The donor 96-well microplate was equipped with GutBox Coated Stirrers (pION Inc.), and filled with buffered solutions of the test compounds (180 μ L per well), in quadruplicates. Each filter membrane on the 96-well acceptor plate was impregnated with 5 μ L of the pION BBB-1 lipid solution (Lot No: 520395). The acceptor plate was filled with Brain Sink buffer (200 μ L per well) and placed on the donor plate. The plate “sandwich” was then stirred with a stirrer (Gut-BoxTM; pION Inc., MA, USA), with stirring set to 60 (aqueous boundary layer thickness, μ m) for 1 h at room temperature. After the incubation, the plates were carefully separated and the absorbance spectra of the blank (Prisma HT buffer, pH 7.40), donor, acceptor, and reference wells were measured with a microplate reader (SynergyTM H4; BioTek Instruments, Inc., VT, USA). The logarithms of the effective permeability ($\log P_e$) were calculated using PAMPA Explorer Software (pION Inc.). Based on the standard compounds, the following ranges of permeability were established: $\log P_e > -5.0$, high permeability (compound can enter the CNS; CNS+); $\log P_e \leq -6.9$, low permeability (compound is excluded from the CNS; CNS-); and $-6.9 < \log P_e \leq -5.0$, permeability uncertain; CNS \pm).

A β ₁₋₄₂ Aggregation Inhibitory Activity Assay

Thioflavin-T (ThT) fluorometric assay [34]. Recombinant human HFIP-pretreated A β ₁₋₄₂ peptide (Merck Millipore, Darmstadt, Germany) was dissolved in DMSO to give a 75 μ M stock solution. The stock solution was further diluted in HEPES buffered solution (150 mM HEPES, pH 7.4, 150 mM NaCl), to 7.5 μ M. A β ₁₋₄₂ solution was then added to compounds **4–8, 14, 15** and **22–25** in black-walled 96-well plates, and diluted with ThT solution (final

concentration, 10 μM). The final mixture contained 1.5 μM $\text{A}\beta_{1-42}$, 10 μM compounds **4–8**, **14**, **15** and **22–25**, and 3% DMSO. ThT fluorescence was measured every 300 s (excitation wavelength, 440 nm; emission wavelength, 490 nm), with the medium continuously shaking between measurements, using a 96-well microplate reader (Synergy™ H4; BioTek Instruments, Inc., USA). The ThT emission from the $\text{A}\beta_{1-42}$ began to rise after 4 h, reached a plateau after 20 h, and then remained almost unchanged for an additional 28 h of incubation. The fluorescence intensities at the plateau in the absence and presence of the test compound were averaged, and the average fluorescence of the corresponding wells at $t = 0$ h was subtracted. The $\text{A}\beta_{1-42}$ aggregation inhibitory potency is expressed as the percentage inhibition ($\% \text{ inh} = (1 - F_i / F_0) \times 100\%$), where F_i is the increase in fluorescence of $\text{A}\beta_{1-42}$ treated with the test compound, and F_0 is the increase in fluorescence of $\text{A}\beta_{1-42}$ alone.

Cell-Based Assays

Cell Culture and Treatments

The human neuroblastoma SH-SY5Y cell line was purchased from American Type Culture Collection (CRL-2266; Manassas, VA, USA). Cells were cultured in Dulbecco's modified Eagle's medium (Sigma, St. Louis, MO, USA) supplemented with 10% fetal bovine serum (HyClone, Logan, UT, USA), 2 mM *L*-glutamine, 50 U/mL penicillin and 50 $\mu\text{g}/\text{mL}$ streptomycin (Sigma, St. Louis, MO, USA) in a humidified atmosphere of 95% air and 5% CO_2 at 37 °C, and grown to 80% confluence. Prior to cell treatment, complete medium was replaced with reduced-serum medium (i.e., with 2% fetal bovine serum). Compounds **6** and **7** were prepared as 20 mM stock solutions in DMSO. For the cytotoxic stimuli, the peptide $\text{A}\beta_{1-42}$ was dissolved in DMSO to a 1 mM stock solution.

Cell Viability Assay

SH-SY5Y cells were seeded in 96-well plates (2×10^4 /well) and assessed using MTS (3-(4,5-dimethylthiazol-2-yl)-5-(3-carboxymethoxyphenyl)-2-(4-sulfophenyl)-2H-tetrazolium, inner salt) assay for the responses of compounds **6** and **7**. The cells were treated with increasing concentrations of compounds **6** and **7** (1–100 μ M), and cell viability was assessed after 48 h using the CellTiter 96[®] Aqueous One Solution Cell Proliferation Assay (Promega, Madison, WI, USA), according to the manufacturer instructions. Absorbance was measured with an automatic microplate reader (Tecan Safire², Switzerland) at a wavelength of 492 nm. Results are presented as a percentages of the control (DMSO).

Neuroprotection Assay

The neuroprotective effects of compounds **6** and **7** on the cytotoxic effect of A β ₁₋₄₂ were assessed using the MTS assay. Prior to cell treatment, the peptide A β ₁₋₄₂ was incubated at a final concentration of 5 μ M, in reduced-serum medium in the absence and presence of 5 μ M compound **6** and 2.5 μ M compound **7**, for 24 h at 37 °C, to induce A β aggregation. SY5Y cells were seeded in 96-well plates (2×10^4 /well), and next day they were treated with pre-aggregated A β ₁₋₄₂ in the absence and presence of the compounds. After 48 h treatment, cell viability was determined using the CellTiter 96[®] Aqueous One Solution Cell Proliferation Assay (Promega, Madison, WI, USA), according to the manufacturer instructions. Absorbance was measured with an automatic microplate reader (Tecan Safire², Switzerland) at a wavelength of 492 nm. The results are presented as percentages of the control (DMSO).

Acknowledgments

This study was supported by the Slovenian Research Agency, the France-Alzheimer Foundation (FA-AAP-2013-65-101349), the Agence Nationale de la Recherche (ANR-12-BS07-0008-03), and Institut Francais. We thank Marielle Vandhammer and Marie Trosvalet

for providing us with lyophilized murine AChE and human BChE, as well as for continuous and fruitful discussions. We thank Julija Lipušček for her contribution. We thank Dr. Dušan Žigon (Jožef Stefan Institute, Ljubljana, Slovenia) for performing the mass spectrometry measurements. We also thank Dr. Chris Berrie for critical reading of the manuscript.

Supporting Information

Supplementary data associated with this article can be found, in the online version, at <http://>.

ACCEPTED MANUSCRIPT

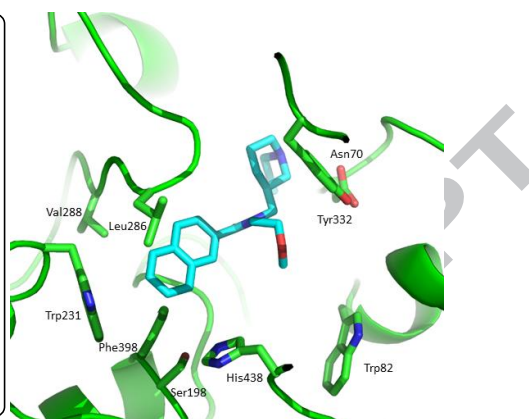
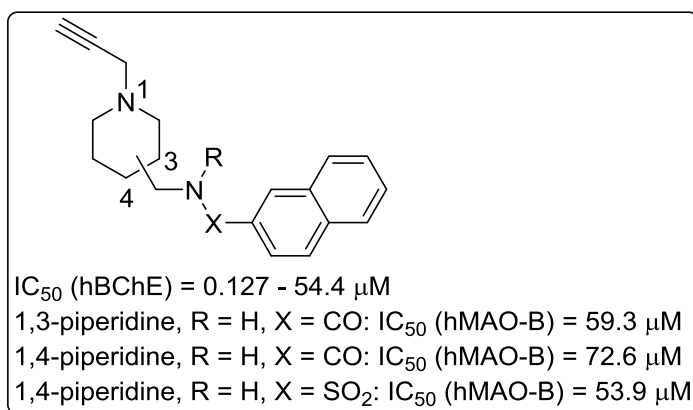
References

- [1] Querfurth, H. W.; LaFerla, F. M. *N. Engl. J. Med.* **2010**, *362*, 329.
- [2] Scherder, E. *Aging and Dementia: Neuropsychology, Motor Skills, and Pain*. VU University Press **2011**, p. 22.
- [3] Scarpini, E.; Schelterns, P. *Lancet Neurol.* **2003**, *2*, 539.
- [4] Perry, E. K.; Tomlinson, B. E.; Blessed, G.; Bergmann, K.; Gibson, P. H.; Perry, R. H. *Br. Med. J.* **1978**, *2*, 1457. –1459.
- [5] Glabe, C. C. in *Subcellular Biochemistry: Alzheimer's Disease: Cellular and Molecular Aspects of Amyloid β* ; Harris, J. R.; Fahrenholz, F., Eds.; Springer, **2005**; Vol. 38, pp 167–177.
- [6] Sugimoto, H.; Iimura, Y.; Yamanishi, Y.; Yamatsu, K. *J. Med. Chem.* **1995**, *38*, 4821.
- [7] Greenblatt, H. M.; Kryger, G.; Lewis, T.; Silman, I.; Sussman, J. L. *FEBS Lett.* **1999**, *463*, 321.
- [8] Bar-On, P.; Millard, C. B.; Harel, M.; Dvir, H.; Enz, A.; Sussman, J. L.; Silman I. *Biochemistry* **2002**, *41*, 3555.
- [9] Benhamú, B.; Martín-Fontecha, M.; Vázquez-Villa, H.; Pardo, L.; López-Rodríguez, M. *L. J. Med. Chem.* **2014**, *57*, 7160.
- [10] Perry, E. K.; Tomlinson, B. E.; Blessed, G.; Bergmann, K.; Gibson, P. H.; Perry, R. H. *Br. Med. J.* **1978**, *2*, 1457.
- [11] Greig, N. H.; Utsuki, T.; Ingram, D. K.; Wang, Y.; Pepeu, G.; Scali, C.; Yu, Q. S.; Mameczarz, J.; Holloway H. W.; Giordano, T.; Chen, D.; Furukawa, K.; Sambamurti, K.; Brossi, A.; Lahiri, D. K. *Proc. Natl. Acad. Sci.* **2005**, *102*, 17213.
- [12] Košak, U.; Brus, B.; Knez, D.; Šink, R.; Žakelj, S.; Trontelj, J.; Pišlar, A.; Šlenc, J.; Gobec, M.; Živin, M.; Tratnjek, L.; Perše, M.; Sałat, K.; Podkova, A.; Filipek, B.;

- Nachon, F.; Brazzolotto, X.; Więckowska, A.; Malawska, B.; Stojan, J.; Mlinarič Raščan, I.; Kos, J.; Coquelle, N.; Colletier, J. P.; Gobec, S. *Submitted for publication*.
- [13] Youdim, M. B. H.; Edmondson, D.; Tipton, K. *Nat. Rev. Neurosci.* **2006**, *7*, 295.
- [14] Binda, C.; Newton-Vinson, P.; Hubálek, F.; Edmondson, D. E.; Mattevi, A. *Nat. Struct. Mol. Biol.* **2002**, *9*, 22.
- [15] Carradori, S.; Silvestri, R. *J. Med. Chem.* **2015**, *58*, 6717.
- [16] Gaspar, A.; Silva, T.; Yáñez, M.; Vina, D.; Orallo, F.; Ortuso, F.; Uriarte, E.; Alcaro, S.; Borges, F. *J. Med. Chem.* **2011**, *54*, 5156.
- [17] Bautista-Aguilera, O. M.; Samadi, A.; Chioua, M.; Nikolic, K.; Filipic, S.; Agbaba, D.; Soriano, E.; de Andrés, L.; Rodríguez-Franco, M. I.; Alcaro, S.; Ramsay, R. R.; Ortuso, F.; Yaněz, M.; Marco-Contelles, J. *J. Med. Chem.* **2014**, *57*, 10455.
- [18] León, R.; Garcia, A. G.; Marco-Contelles, J. *Med. Res. Rev.* **2013**, *33*, 139.
- [19] Bajda, M.; Guzior, N.; Ignasik, M.; Malawska, B. *Curr. Med. Chem.* **2011**, *18*, 4949.
- [20] Brus, B.; Košak, U.; Turk, S.; Pišlar, A.; Coquelle, N.; Kos, J.; Stojan, J.; Colletier, J. P.; Gobec, S. *J. Med. Chem.* **2014**, *57*, 8167.
- [21] Lipinski, C. A.; Lombardo, F.; Dominy, B. W.; Feeney, P. J. *Adv. Drug Deliv. Rev.* **2001**, *46*, 3–26.
- [22] Samadi, A.; de los Ríos, C.; Bolea, I.; Chioua, M.; Iriepa, I.; Moraleda, I.; Bartolini, M.; Andrisano, V.; Gálvez, E.; Valderas, C.; Unzeta, M.; Marco-Contelles J. *Eur. J. Med. Chem.* **2012**, *52*, 251.
- [23] Ciapetti, P.; Giethlen, B. in *The Practice of Medicinal Chemistry*; Wermuth, C. G., Ed. Academic Press **2008**, pp 290–342.
- [24] Rankovic, Z. *J. Med. Chem.* **2015**, *58*, 2584.
- [25] Košak, U.; Brus, B.; Gobec, S. *Tetrahedron Lett.* **2014**, *55*, 2037.

- [26] Knez, D.; Brus, B.; Coquelle, N.; Sosič, I.; Šink, R.; Brazzolotto, X.; Mravljak, J.; Colletier J. P.; Gobec, S. *Bioorg. Med. Chem.* **2015**, *23*, 4442.
- [27] Tsou, H. R.; Mamuya, N.; Johnson, B. D.; Reich, M. F.; Gruber, B. C.; Ye, F.; Nilakantan, R.; Shen, R.; Discafani, C.; DeBlanc, R.; Davis, R.; Koehn, F. E.; Greenberger, L. M.; Wang, Y. F.; Wissner A. *J. Med. Chem.* **2001**, *44*, 2719.
- [28] Ellman, G. L.; Courtney, K. D.; Andres jr., V.; Featherstone, R. M. *Biochem. Pharmacol.* **1961**, *7*, 88.
- [29] Kryger, G.; Harel, M.; Giles, K.; Toker, L.; Velan, B.; Lazar, A.; Kronman, C.; Barak, D.; Ariel, N.; Shafferman, A.; Silman, I.; Sussman, J. L. *Acta Crystallogr. D Biol. Crystallogr.* **2000**, *56*, 1385.
- [30] Rankovic, Z. *J. Med. Chem.* **2015**, *58*, 2584.
- [31] Meyer-Luehmann M.; Spires-Jones, T. L.; Prada, C.; Garcia-Alloza, M.; de Calignon, A.; Rozkalne, A.; Koenigsnecht-Talboo, J.; Holtzman, D. M.; Bacskai, B. J.; Hyman, B. T. *Nature* **2008**, *451*, 720.
- [32] Wolfe, M. S. *Nat. Rev. Drug. Discov.* **2002**, *1*, 859.
- [33] Citron, M. *Nat. Rev. Drug. Discov.* **2010**, *9*, 387.
- [34] LeVine 3rd, H. *Protein Sci. Publ. Protein Soc.* **1993**, *2*, 404.
- [35] The number of signals in ^{13}C NMR exceeds the number of carbon atoms, due to ring inversion and N-inversion at room temperature, which leads to conformational isomers.
- [36] von der Eltz, H.; Guder, H. J.; Muhlegger, K. USP Patent No. 4900822, Feb. 13, 1990.
- [37] Brazzolotto, X.; Wandhammer, M.; Ronco, C.; Trovaslet, M.; Jean, L.; Lockridge, O.; Renard, P. Y.; Nachon, F. *FEBS J.* **2012**, *279*, 2905.
- [38] Kabsch, W. *Acta Crystallogr. D Biol. Crystallogr.* **2010**, *66*, 125.
- [39] McCoy, A. J.; Grosse-Kunstleve, R. W.; Adams, P. D.; Winn, M. D.; Storoni, L. C.; Read, R. J. *J. Appl. Crystallogr.* **2007**, *40*, 658.

- [40] Adams, P. D.; Afonine, P. V.; Bunkóczi, G.; Chen, V. B.; Davis, I. W.; Echols, N.; Headd, J. J.; Hung, L. W.; Kapral, G. J.; Grosse-Kunstleve, R. W.; McCoy, A. J.; Moriarty, N. W.; Oeffner, R.; Read, R. J.; Richardson, D. C.; Richardson, J. S.; Terwilliger, T. C.; Zwart, P. H. *Acta Crystallogr. D Biol. Crystallogr.* **2010**, *66*, 213.
- [41] Emsley, P.; Lohkamp, B.; Scott, W. G.; Cowtan, K. *Acta Crystallogr. D Biol. Crystallogr.* **2010**, *66*, 486.
- [42] Schüttelkopf, A. W.; van Aalten, D. M. F. *Acta Crystallogr. D Biol. Crystallogr.* **2004**, *60*, 1355.



ACCEPTED MANUSCRIPT

HIGHLIGHTS

- New multifunctional propargylamines were synthesized and evaluated biologically.
- All compounds selectively inhibit human butyrylcholinesterase.
- All compounds cross the blood-brain barrier in an *in vitro* assay.
- Three compounds also inhibit monamine oxidase B.
- The crystal structure of human butyrylcholinesterase in complex with **3** was solved.

ACCEPTED MANUSCRIPT